Robot Gripper Control System Using PVDF Piezoelectric Sensors

by

Michael F. Barsky

Thesis submitted to the Faculty of the
Virginia Polytechnic Institute and State University
in partial fulfillment of the requirements for the degree of
Master of Science
in
Department of Electrical Engineering

APPROVED:

Richard O. Claus, Chairman

Douglas K. Lindner

John W. Roach

Nelson N. Hsu

Steven E. Fick

May, 1986

Blacksburg, Virginia

Robot Gripper Control System Using PVDF Piezoelectric Sensors

by

Michael F. Barsky

Richard O. Claus, Chairman

Department of Electrical Engineering

(ABSTRACT)

A novel robot gripper control system is presented which uses PVDF piezoelectric sensors to actively damp exerted force. By using a low-input-resistance amplifier to sense the current developed by the PVDF sensor, an output proportional to the rate of change of the force exerted by the gripper is obtained. The signals from the PVDF sensor and a strain gauge force sensor are arranged in a proportional and derivative (PD) control system for the control of force. The control system was tested on an instrumented Rhino XR-1 manipulator hand. The capabilities of the control system are analyzed analytically, and verified experimentally. The results for this particular gripper indicate that as much as 900% improvement in force step response rise time, and 300% reduction in overshoot are possible by inclusion of the PVDF sensor.

ACKNOWLEDGEMENTS

I would like to thank each member of my committee for their contributions and support of my project. Special thanks are owed to Dr. Hsu, Dr. Fick, and the rest of the Ultrasonic Standards Group at the National Bureau of Standards for their technical and financial assistance.

Thanks goes to fellow graduate student Karl Reichard who assisted in the design and construction of the sensor. I would like to thank Dinah Akers for her assistance in preparing the manuscript, and Robin Rogers for drawing many of the figures. Also, thanks goes to all who read early drafts of the manuscript. These include my committee members, my brother Daniel, and fellow graduate student Mark Maggenti. Finally, I would like to thank my family for their constant support and encouragement. I would like to dedicate this thesis in memory of my grandfather, Abraham Calisoff, who inspired me to become an engineer.

TABLE OF CONTENTS

LIST OF ILLUSTRATIONS

CHAPTER I. INTRODUCTION

Polyvinylidene fluoride (PVDF) is a piezoelectric polymer displaying great promise for use in sensors for robot systems. In this thesis, a novel use of this material for robot gripper control is presented. A piezoelectric sensor functions as a rate-of-force sensor for derivative feedback, while a strain gauge senses the integrated force exerted upon the entire gripping surface. The sensors are used together in a proportional and derivative (PD) control system. The benefits afforded by the addition of rate feedback are evaluated by comparing the performance of a gripper with and without the piezoelectric sensor.

This project was motivated by the trend in industry toward sensory feedback robotics. Sensory feedback promises smarter robots capable of self-correction, high accuracy, and increased speed. Recent efforts in tactile sensing for the purpose of controlling general purpose end-effectors was particularly motivational for this project. There are many interrelated problems in this developing field [3]. For example, it would be desirable to integrate tactile sensing and vision systems or other sensor systems under hierarchial control to achieve optimal performance in operations such as picking and placing. In this paper, a similar type of integration is pursued for the purpose of demonstrating how two

sensors working together to sense the same variable can achieve superior overall performance.

One problem that is infrequently mentioned in tactile sensor research is the problem of stability. In control engineering, stability and feedback are always considered simultaneously. In an effort to design robots to operate more quickly and with decreased error in controlled parameters, the loop gains in the sensor feedback control systems will be raised to the limit of stability. In this thesis, a sensor and control technique are presented which, in theory, could do for robot gripper force control what tachometers do for satellite tracking radar: provide active damping to expand the range of stable performance.

Robot gripper control throughout this paper is the control of the force integrated over the gripping area. The integrated force is directly relevant to the important issue of gripper compliance control, because if the force is controlled, and the loop gain is specified, then a particular degree of compliance will result. If the additional feedback reduces the response time to errors in the desired force, then it also expands the range of compliance. Therefore, without loss of generality, all results are presented in terms of response time. Furthermore, control in terms of force alone (as opposed to force and position, for example) sharply focuses attention on the benefits provided by piezoelectric sensory feedback. Compliance control could

also be defined in terms of the finger position and velocity [1], or in terms of both force and position [2]. Gripper control in general may also depend on static variables such as object orientation. Orientation tactile sensors are a topic of vigorous research [3-7].

In crude experiments, the PVDF transducer was found to be troublesome for absolute force feedback due to output drift and temperature sensitivity; others have reported similar findings [6]. Still others claim that the use of extremely thin piezoelectric films [8,9], and temperature compensation [10], may make piezoelectric sensors practical for absolute force measurements. Piezoelectrics, however, function quite naturally as rate-of-force sensors. Force rate sensing is naturally robust because all transient disturbances decay exponentially. No charge amplification or high input impedance voltage amplifiers are required. One must simply measure the current output of the transducer using a low input impedance amplifer. If a piezoelectric sensor and an integrated force sensor are used together, force and damping will be simultaneously controllable as in a classical PD control system where the position variable is force, and the velocity variable is rate-of-force.

The control problem discussed here is to maximize the rise time of a step change in force under the constraint of zero overshoot. The problem is specified in terms of step-response rise time and overshoot because the most demanding

gripper applications require fast response time and generally cannot tolerate overshoot. The step function is the most difficult function encountered in practice, and the most practical in view of speed maximization. The step-response analysis throughout this thesis is confined to transitions between approximately 0.5N and 3N of force. In addition, experimental results are reported which demonstrate the possibility of extending the results to the control of nonlinear impact forces.

The next chapter describes the experimental apparatus. The third chapter describes the modelling techniques and presents transfer function models for the gripper and the piezoelectric sensor. The fourth chapter describes the results of the theoretical and experimental work which made use of the models and apparatus developed in the previous sections. The fifth chapter is a discussion of some possible areas for further research. The last chapter summarizes the results.

CHAPTER II. EXPERIMENTAL APPARATUS

The goal of this investigation was to evaluate the capabilities of the rate feedback control system both analytically, and by experiment. Robot gripper models reported in the literature are not suitable for this purpose because the actual grippers described are not readily available. Instead of using previously established gripper models, a gripper was selected (mostly on the basis of availability), independently modelled, and analyzed. In this chapter, the equipment assembled and built is described in detail.

The robot gripper, sensors, and control system are represented in the block diagram shown in Figure 1. The transfer function G(s) =(Output Force)/(Input Voltage) represents the dynamic coupling between the input voltage to the device comprised of a pulse-width-modulated power amplifier, DC permanent magnet motor, robot gripper mechanism, and force sensor, and the force exerted by the gripper. The pulsed power amplifier is required to boost the signal power and reduce nonlinearities introduced by commutator voltage drop in the drive motor. The piezoelectric force sensor is represented by the transfer function P(s)=(Output Voltage)/(Input Force). The gains K and ℓ are the scalar feedforward and rate feedback gains, respectively.

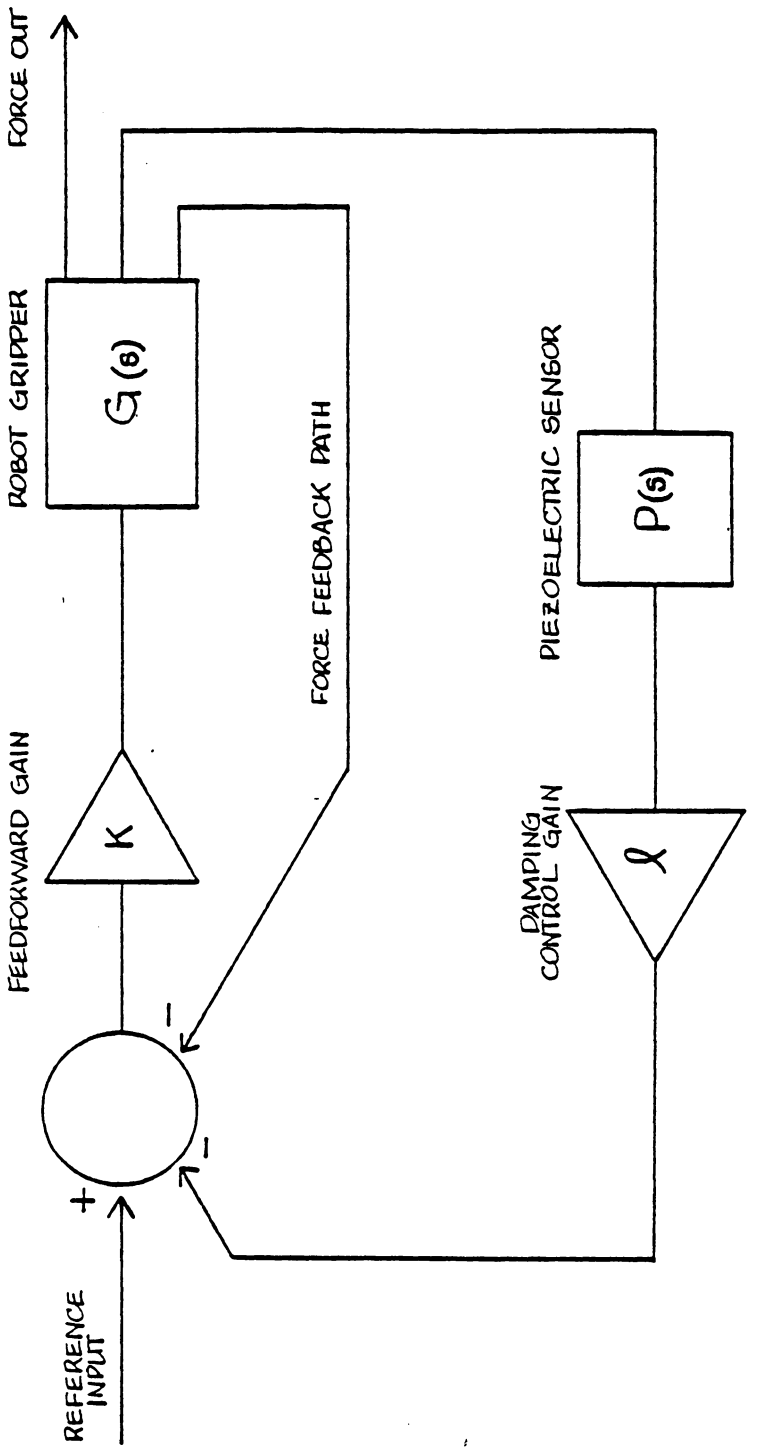

Figure 1. Block Diagram of the Control System.

2.1 GRIPPER DESCRIPTION

The gripper on a Rhino XR-1 manipulator, selected for this experiment, is similar in design to many popular industrial grippers. It consists of a DC motor, gear box, and mechanical linkages. The gear box isolates forces exerted on the gripping surfaces from the motor. As a result, deactivating the motor causes the gripper jaws to lock in position. Position-locking grippers tend to be more energy efficient than back-drivable grippers (gripper mechanisms without gear boxes between the motor and linkages) where steady-state forces are not isolated from the drive motor. The fact that steady-state forces are isolated from the the drive motor removes the option of force control through current monitoring at the drive motor. The Rhino gripper also has about 0.2 radians of backlash due to the gear box and linkages. This amount of backlash is significant, as will be discussed in subsequent chapters.

2.2 FORCE SENSOR

The instrumented fingers of the gripper are shown with mounted sensors in Figure 2. Only one piezoelectric and one force sensor are necessary for the experiment because the gripper applies forces symmetrically to both fingers. This configuration is suitable for the present experiment. The

practical implementation of this concept may require more sensors, as discussed in chapter 5. The force sensor is a Transensory Devices[1] TP 4010 silicon strain gauge. It was selected for its excellent linearity, low hysteresis, absolute accuracy, fast response time and commercial availability.

2.3 PIEZOELECTRIC FORCE-RATE SENSOR

The polymer PVDF is an ideal piezoelectric for rate-of-force sensing because of its strong low-Q response, ease of use, and high compliance; properties which are lacking in most non-polymeric piezoelectrics. Techniques used to etch electrode patterns on the film are described in [11]. The sensor is mechanically designed to reject stretch-mode response, while allowing thickness-mode (compression) response. All but a small circular spot of conductor is etched away on one side of a rectangular piece of PVDF film, as shown in Figure 3a. The opposite side of the film is completely covered by the conductor. The inner conductor of a short piece of small-diameter coaxial cable is connected to the

---

[1] Certain commercial products are identified in this document to adequately identify the system. Such identification does not imply recomendation or endorsement by the National Bureau of Standards or VPI&SU, nor does it imply that the materials or equipment identified are necessarily the best available for the purpose.

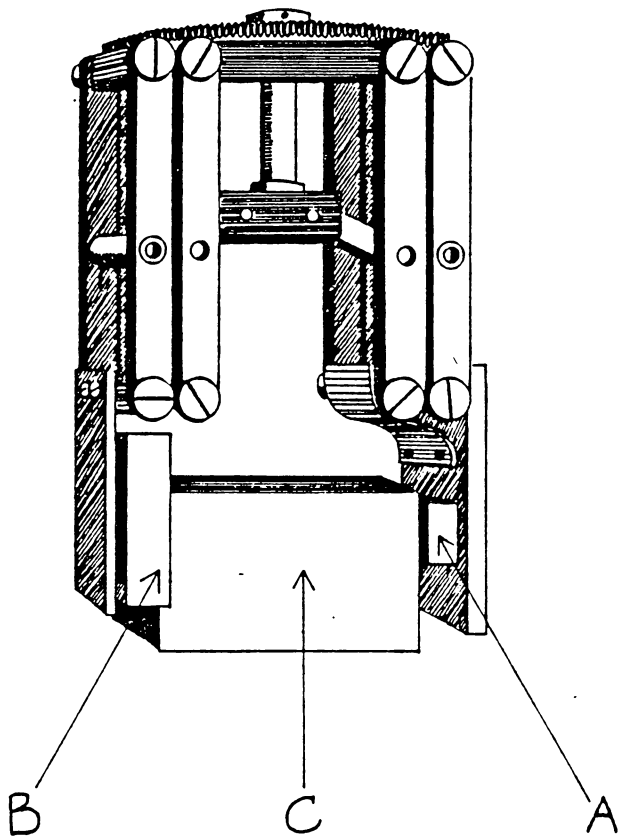

Figure 2. Instrumented Robot Gripper: a) force sensor, b) piezoelectric rate-of-force sensor, c) object under force.

conducting spot using conductive epoxy. One edge of the film is bent upward, and the outer conductor of the coax is attached to the front surface at the bend. Finally, the sensor is potted in non-conducting epoxy with the conducting surface of the film facing outward as shown in Figure 3b. The coaxial cable and grounded front surface provide excellent shielding, while the potting epoxy provides support for the cable connection and the film. This construction technique is a modification of the technique described by Dario for piezoelectric array sensors [6]. Dario's technique, however, requires a special feed-through circuit board for support and electrical connection. A complete description of the construction process is included in the appendix.

The coaxial cable from the sensor is connected to a nearby amplifier which buffers the voltage signal across a 1 megohm input resistor. The capacitance of the film is approximately 10 pF. The input resistor and this capacitance form a first-order bandpass network with a resonant frequency of approximately 20 kHz. Since the step response rise time of the sensor is 20 microseconds, the bandwidth of the bandpass network is only slightly wider than that of the sensor. This band-limiting damps high-frequency noise, but also places an upper limit on the rate at which the force can change if it is to be detected accurately. The wide bandwidth of the piezoelectric sensor is of key importance in its application as a rate-of-force sensor. Some force sensors, for instance,

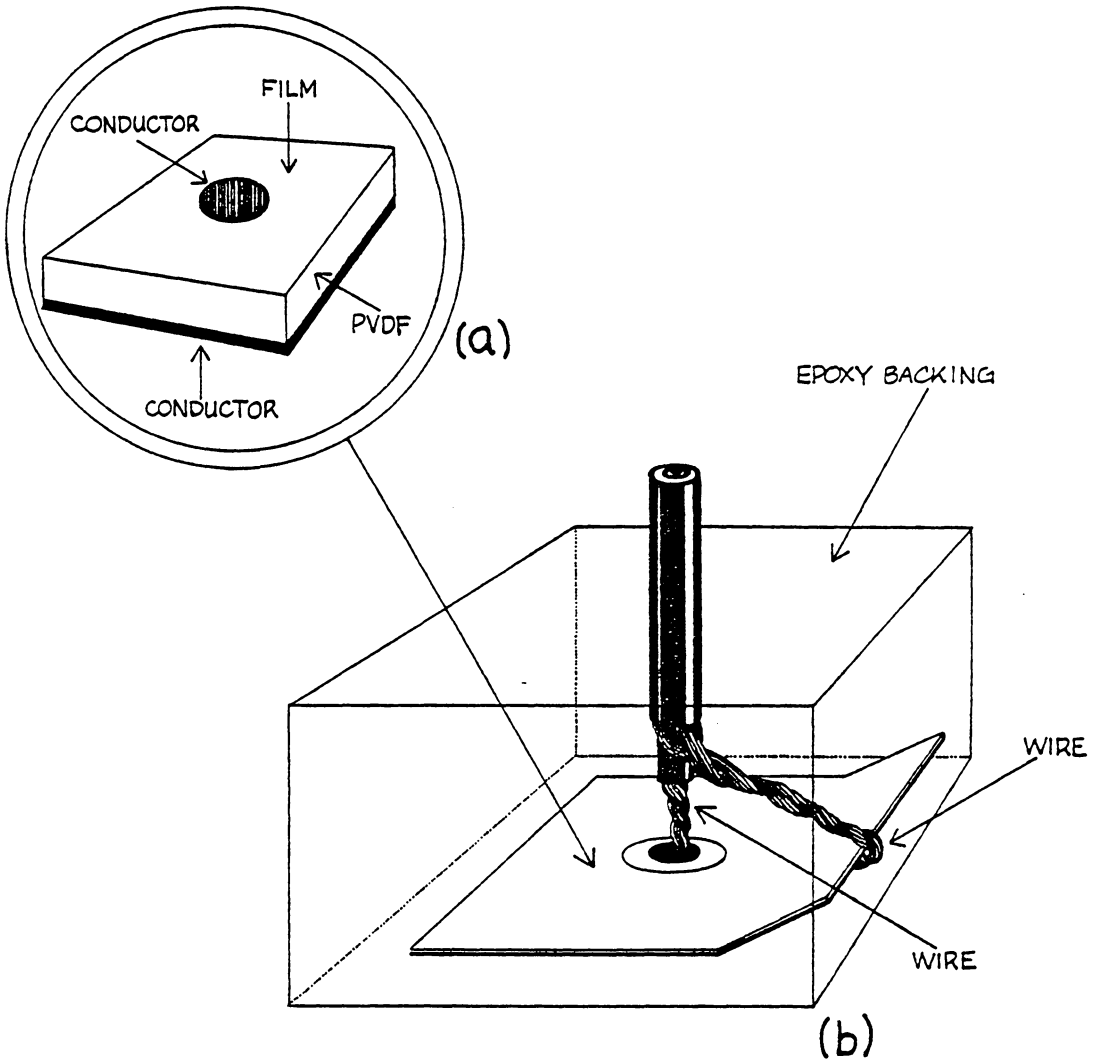

Figure 3. Construction of Piezoelectric Sensor: a) detail of the PVDF film after etching, b) final product.

lack the necessary bandwidth for effective differentiation, regardless of noise issues [3].

2.4 CONTROL ELECTRONICS

A block diagram of the electronic subsystems is shown in Figure 4. The block diagram identifies eleven subsystems, and their relationships with the drive motor, the linkage elements, and the gripper and sensors. The drive motor and linkage elements were purchased as part of the Rhino robot, and were used unchanged from the manufacturer. The sensors were described in the preceeding sections. In this section, the eleven subsystems are briefly described.

All of the circuits are wired on protoboards to facilitate debugging. The protoboards are mounted firmly in an aluminum box which is stacked on top of an identical chassis containing a power supply which provides unregulated +20 and -20 volt, 1 amp lines which are regulated on the circuit boards for use by the signal-processing components. Also supplied are four ground lines for single point grounding, and a regulated 0-15 volt line capable of supplying 1.5 amps to drive the dc electric drive motor. A 10 ohm resistor (supplied by the robot manufacturer) in series with the motor ensures that the power rating of the supply is sufficient.

Proceeding clockwise around Figure 4, the first block is the reference step input function generator. This subsystem

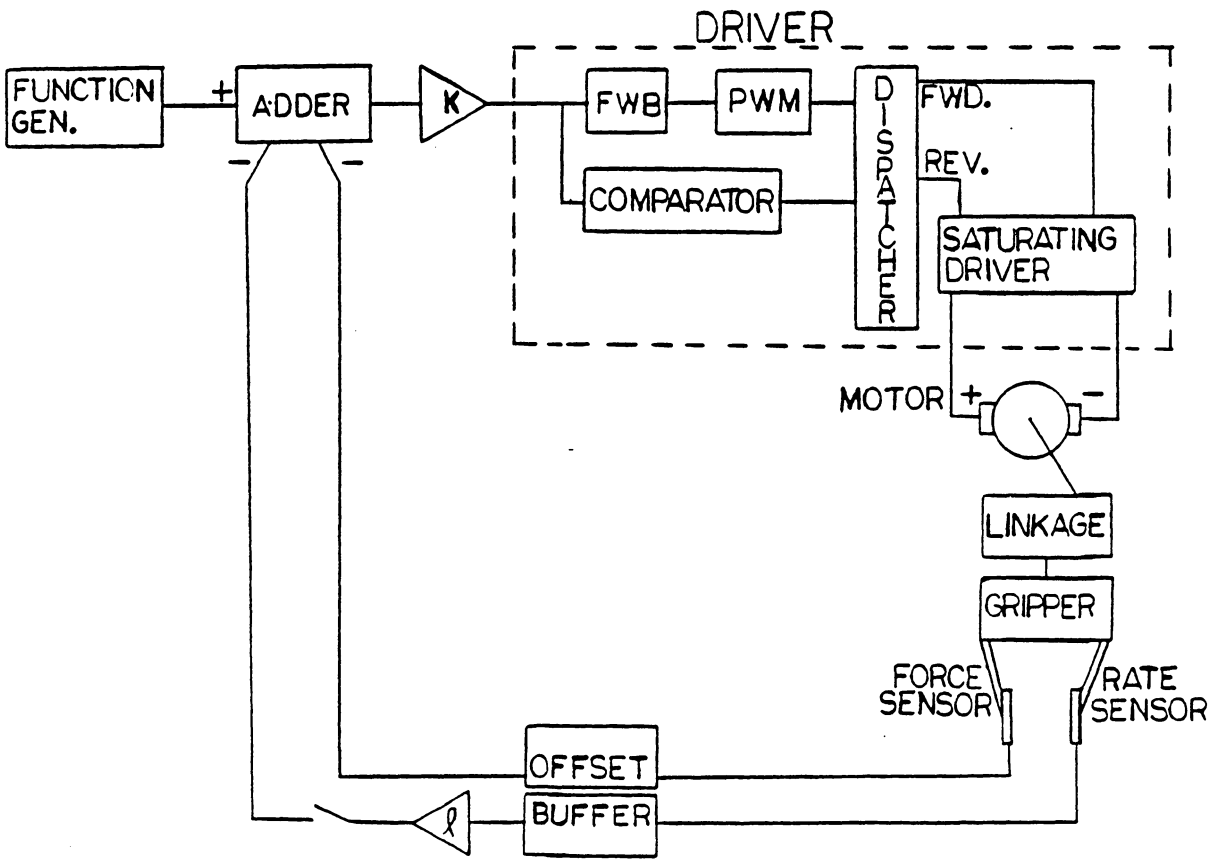

Figure 4. Control Electronics Subsystem Block Diagram

is shown schematically in Figure 5. The switch is debounced using two cross-coupled NAND gates which form an RS flip-flop. The Q output of the flip-flop is either 5 volts or 0 volts with no overshoot, and the settling time is much less than a microsecond. The Q output is attenuated by a factor of 100 using the 20k-200 ohm resistive ladder. This results in a 0-50 mV step function. The op-amp is used to buffer, invert, and offset the step. The final output from the op-amp is a step function from -10mV to -60 mV. The force sensor has a gauge factor of 44 mV/N. Thus, this input function corresponds to a step transition from 0.45 N to 2.7 N. The initial offset force is required to maintain linearity in the experiments. Since the maximum force exertable by the gripper is 25 N, this step transition is relatively small.

The next subsystem is the adder. The circuit used is the standard realization shown in Figure 6. The output of the adder is the difference between the reference signal and the sum of the force and rate-of-force signals.

The feedforward gain is provided by two noninverting amplifiers whose gain product is K, as shown in Figure 7. The cascade connection reduces the offset problem involved in amplifying small signals, and maintains the gain-bandwidth of the individual amplifiers at a low level. The value of K sets the stiffness of the force control. Increasing the value of K has the effect of causing the system to react more quickly to changes in the input, and changes due to disturb-

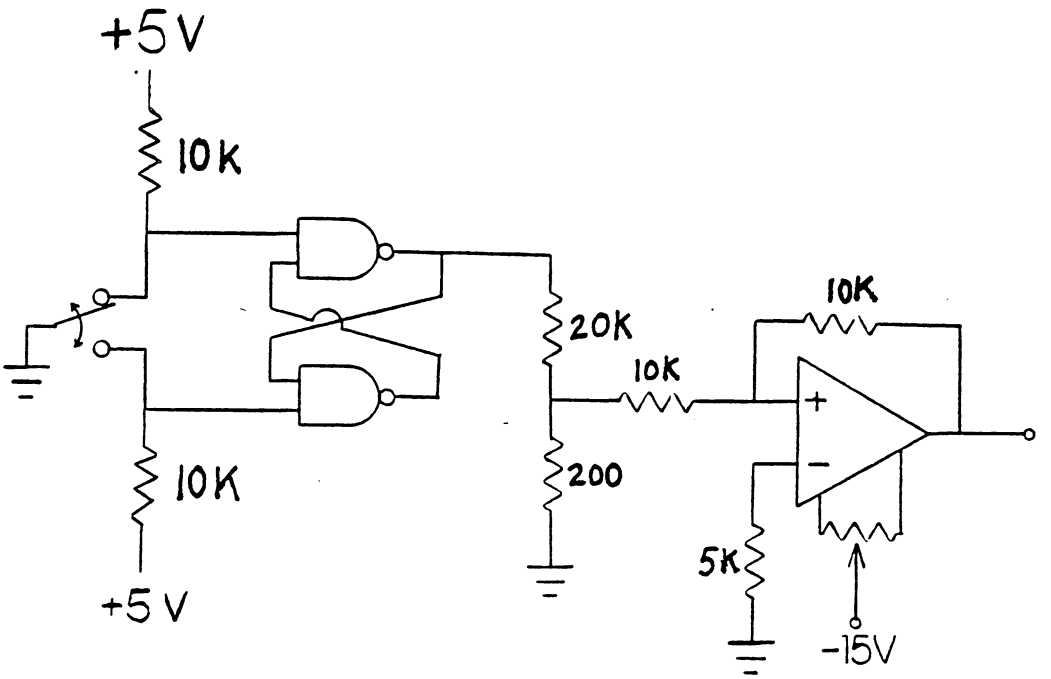

Figure 5. Reference Input

ances. Thus, increasing K improves the system response time, but also tends to destabilize the system. Systems which can tolerate large values of K (that is, sytems which remain stable for large K), are said to have a wide range of stiffness or impedance control.

The output of the feedforward gain stage is applied to the motor after further conditioning by the pulse width modulator (PWM) and pulse amplifier circuitry shown inside the dashed box of Figure 4. The gripper characteristics which require the use of pulse width modulation are explained in the next chapter.

The full-wave bridge (Figure 8), comparator (Figure 9), and dispatcher (Figure 10) are required because the PWM can only modulate unipolar signals. The full-wave bridge generates a unipolar analog input signal signal for the PWM. The PWM output is applied to a "dispatcher" circuit which routes the TTL pulses from the PWM to one of two outputs, depending on the polarity of the output signal from the feedforward gain stage. The polarity is detected by the comparator circuit, which also drives the "dispatcher".

The circuit used for the PWM is shown in Figure 11. This subsystem is based on two 555 timer chips. The chip on the left acts as a clock, providing input pulses at the rate of 200 Hz, and duration 100 ms, to the second 555 which does the pulse-width modulation. The PWM design is similar to the design given by the chip manufacturer [12], with the excep-

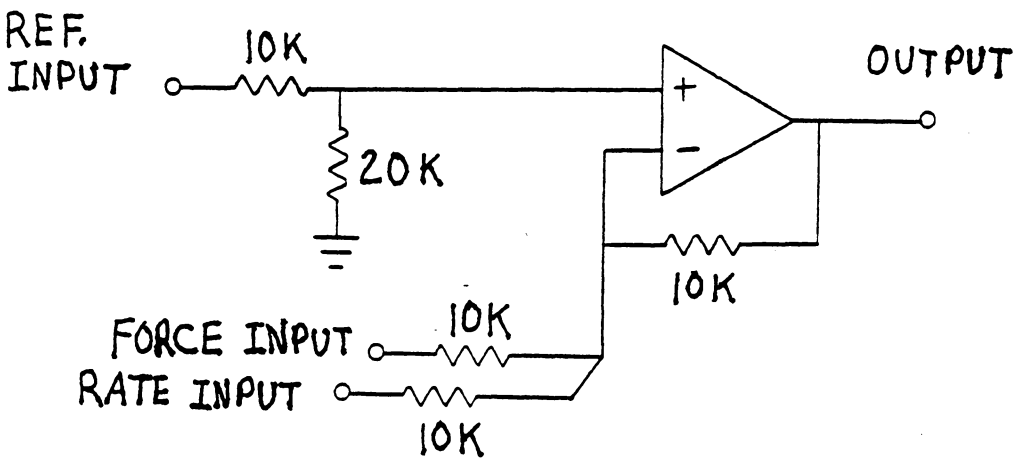

Figure 6. Adder

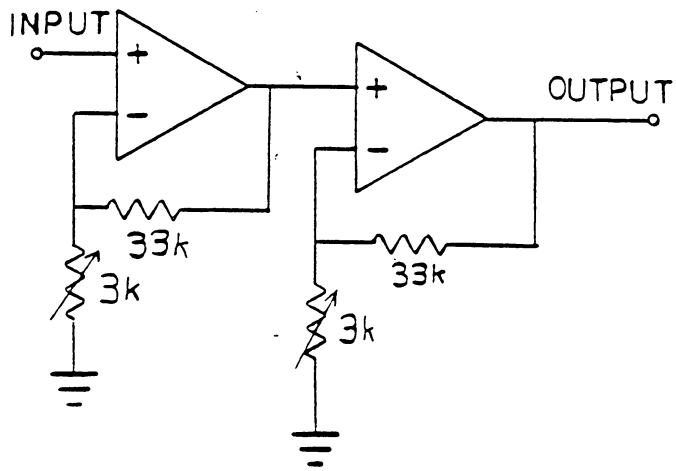

Figure 7. Feedforward Gain

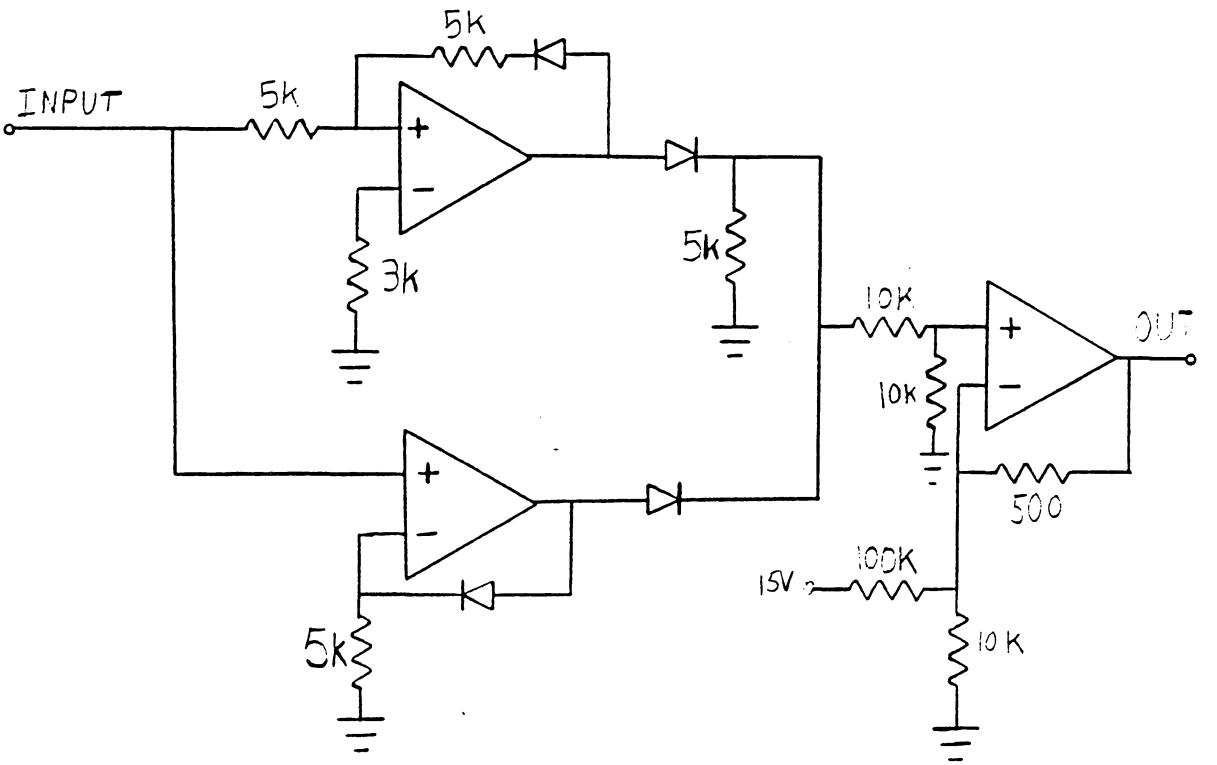

Figure 8. Full-Wave Bridge

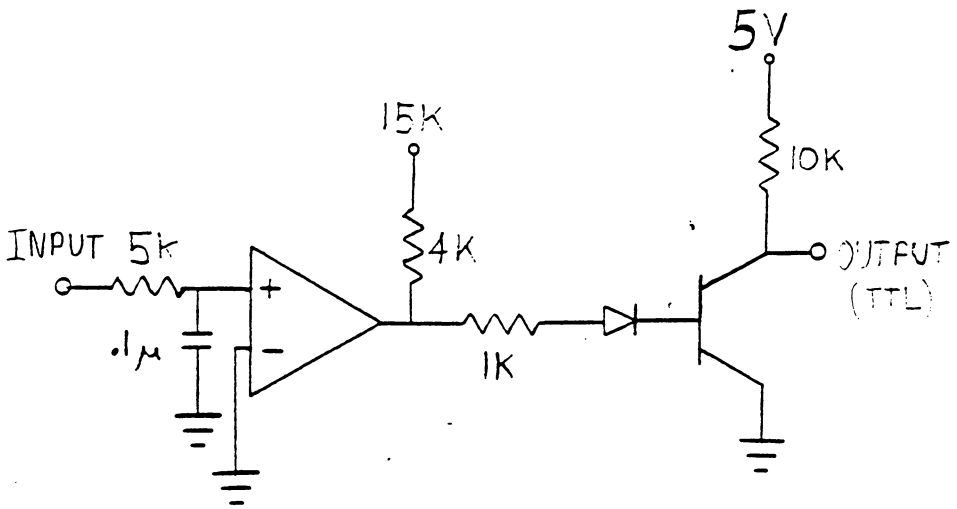

Figure 9. Comparator

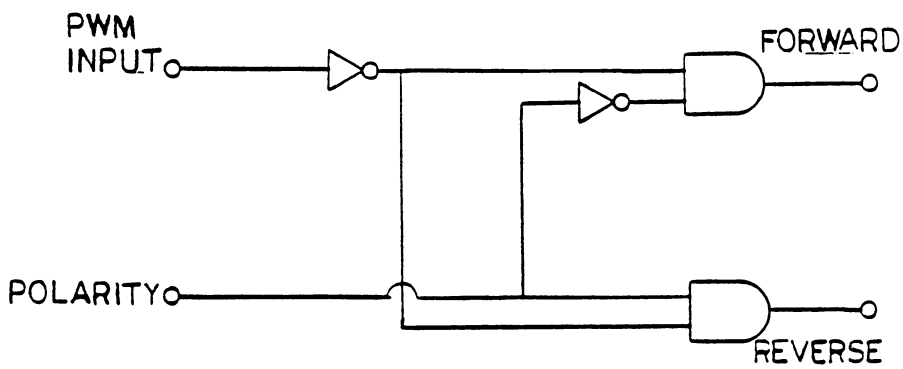

Figure 10. Dispatcher

tion of the transistor Q1 connected to timing capacitor C1. The manufacturer's circuit uses a single resistor from the 15-volt power line to the capacitor. The reason for using the transistor circuit is apparent after a quick analysis of the operation of the PWM. The output of the PWM is set (to 15-volts) as each clock pulse arrives. Simultaneously, the short circuit across the capacitor (provided by a transistor internal to the 555) is removed so that the timing capacitor, C1, may begin to charge. The capacitor voltage increases at a rate determined by the time constant of the resistor (replaced by Q1 and associated circuitry) and the capacitor C1. The capacitor voltage is compared to the amplitude of the input signal (from the feedforward gain amplifier), and the output of the PWM is reset (set to 0-volts) when the capacitor voltage rises above that of the input. The internal transistor discharges and holds the timing capacitor shorted until the next clock pulse arrives. The idea is to get a pulsed output with the duration of the pulses proportional to the amplitude of the input signal. Unfortunately, the charging of a capacitor in an RC network is not linear in time, so that a direct (linear) proportionality would not result if a simple resistor were used. This is the reason for the transistor Q1. The transistor acts as a constant current source which allows the capacitor to charge linearly. The current is approximately one diode drop (0.7 V) divided by the resistance of Re. The resistance is selected so that

a full scale input signal will yeild pulses of nearly 100% duration between clock pulses. The PWM is followed by transistor Q2 to convert the output pulses to TTL levels for the dispatcher.

The dispatcher (Figure 10) has two outputs. Depending on the polarity of the input to the PWM, one output will be inactive, while the other output will carry the train of pulses from the PWM. The line which is inactive and the line which carries the train depends on the output from the comparator. The comparator detects the polarity of the continuous control signal. The outputs from the dispatcher drives the saturating driver which is connected to the motor. The saturating driver (Figure 12) is a bridge-type amplifier using four power transistors, Q1-Q4. This circuit allows the motor to be driven in both directions, without the need for a bipolar power supply. The additional transistors, Q5-Q7, are required to boost the base current for the power transistors.

The loop is then completed by the force sensor offset circuitry, and the rate sensor buffer and gain. The force sensor offset circuitry (Figure 13) is required because the output of the force sensor has a 2.5-volt bias. The force rate sensor buffer and gain circuit is shown in Figure 14. The input resistor on the buffer amplifier determines the bandwidth of the sensor, as was discussed in section 2.3.

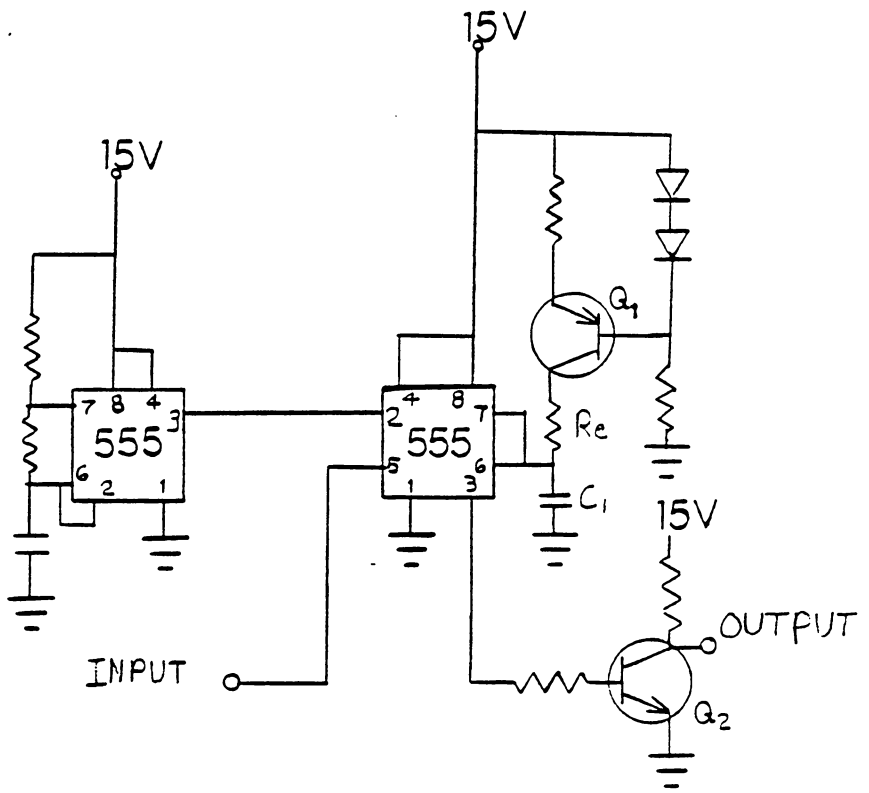

Figure 11. Pulse-Width Modulator

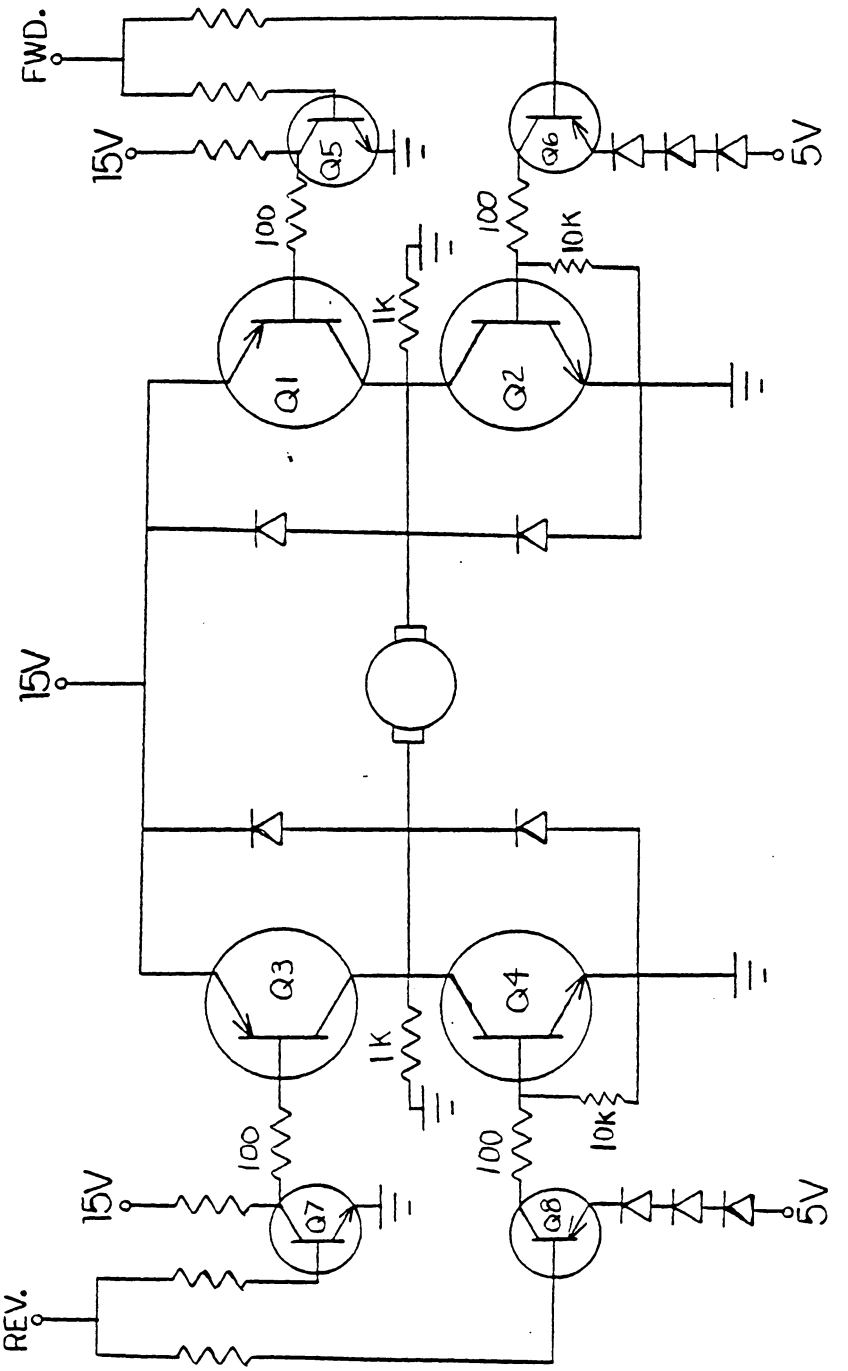

Figure 12. Bridge Amplifier

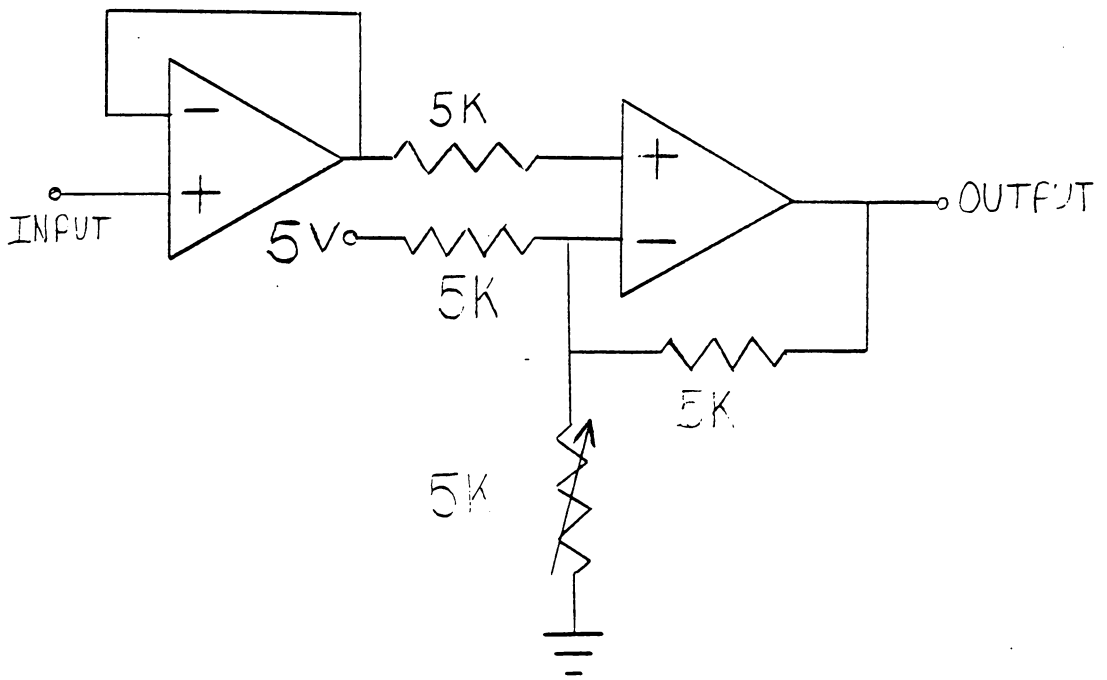

Figure 13. Force Sensor Offset

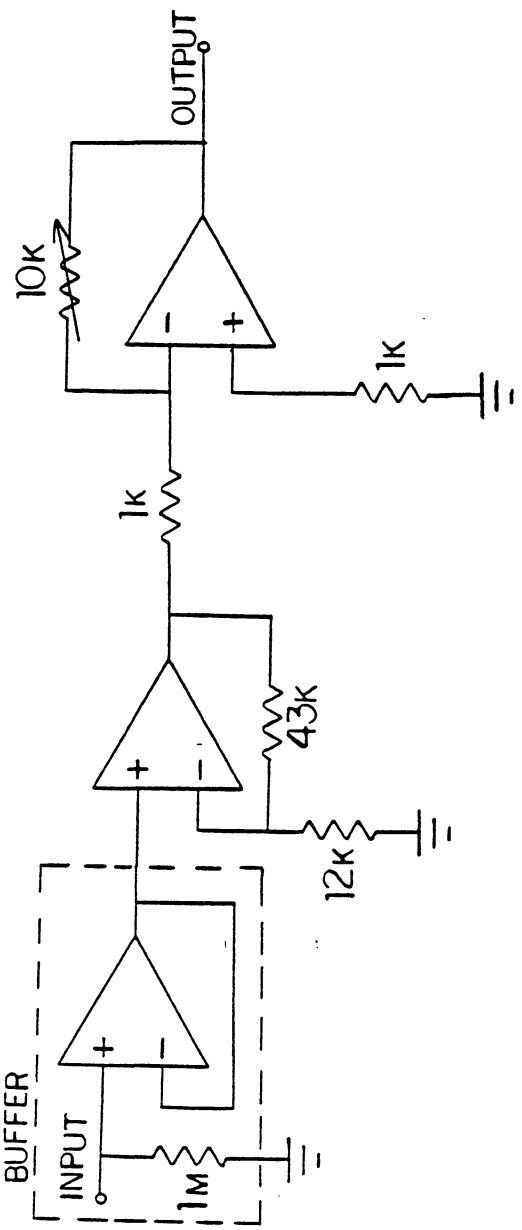

Figure 14. Rate Sensor Buffer Amplifier

CHAPTER III. MODELLING

In this chapter, models of the system are derived for use in the performance simulation presented in Chapter 4. As in any modelling process, the objective is to obtain the simplest adequate mathematical description of the response of the system to all forseeable inputs. Frequency domain transfer function models are selected because transfer functions provide a convenient means of calculating both the time domain closed-loop responses, and frequency domain behavior such as root loci. For these models to be useful, the system must be linear and time invariant. The condition of time-invariance is reasonable for this system, but linearity cannot be guaranteed because there exists saturation in the motor, and backlash in the gearbox. Nevertheless, linear transfer function models are used exclusively. The use of possibly inadequate models increases the need for experimental confirmation of all results predicted by simulation. Discrepencies between simulated and actual results must be explained. In the following sections, models are given for the open-loop system, and for the rate sensor. The open-loop system (labeled G(s) in Figure 1) is the series connection of all of the subsystems presented in the previous chapter, except for the adder, feedforward gain, and components associated with the rate sensor. The rate sensor model includes

the buffer amplifier, but does not include the rate feedback gain.

3.1 OPEN-LOOP SYSTEM IDENTIFICATION

In this section, an output force to input voltage transfer function model for the open-loop system, G(s), is obtained to permit the evaluation of the theoretical closed-loop performance. The preferred technique for identifying a system by its transfer fuction is to estimate pole and zero locations from the magnitude and phase plots of the system. Frequency tests, however, depend heavily of the assumption of system linearity. Since the gripper contains two significant nonlinearities (gearbox backlash and motor saturation), a modelling technique which is not affected by the nonlinearities is required. One such technique is to characterize the system by its step response. The step response test avoids the effects of the backlash nonlinearity because the gearbox operates in only one direction. Simulation using such a model should accurately describe the system performance when there is no overshoot, if an antibacklash gear box is assumed, and approximate the response of the given system when overshoot occurs. The second type of nonlinearity in the system, motor saturation, is circumvented by using certain closed-loop tests, and assuming that the loop gain is sufficiently high. These assumptions will be made precise.

Admittedly, it would be desirable to include the nonlinearities in the analysis, but the results found using the linear model obtained from the step response are suitable to demonstrate the capabilities of the PD control system. To this end, a backlash free ideal model is not unreasonable.

Before presenting the modelling procedure, a brief digression into practical considerations is useful. In chapter 2, a PWM power amplifier was described. If a continuous power amplifier such as the amplifier shown in Figure 15 is used to drive the motor, the dc response shown in Figure 16 results. This response is clearly inadequate because of the 2-volt dead zone, which would cause the closed-loop system to have a large steady state error, or become unstable. The purpose of this investigation is to develop a technique for applying forces quickly and accurately. Therefore, the existence of a source of steady state error must be removed if possible. The solution to this problem was found by analyzing the causes of the dead zone. After reviewing textbooks on electric motors [13], and observing the system in action, two possible causes were isolated. The first was commutator voltage drop, which occurs at the brush-armature connection as a results of oxide build-up on the copper. The second possible source is static friction, which is present throughout the mechanical system. The solution is the use of a PWM power amplifier. The PWM pulses the motor at full rated voltage, causing the commutator voltage drop to become

insignificant. In addition, the bursts of power jerk the motor into action, removing the problem of static friction. The dc response of the system using the PWM power amplifier is shown in Figure 17. This figure shows that the PWM has removed the dead zone.

Closed-loop experiments on the system indicate that two additional assumptions can be made. First, the system can track step inputs without steady-state error. This indicates that the system is at least type 1. Secondly, the system is capable of closed-loop instability. The feedforward gain level which causes instability was measured experimentally. This indicates that the order of the denominator of the transfer function should be at least three orders of magnitude higher than the numerator. Thus, the model should be of the form shown in (1).

$$G(s) = \frac{k(s+a_1)(s+a_2)\ \ldots\ (s+a_n)}{s(s+b_1)(s+b_2)\ \ldots\ (s+b_{n+3})} \qquad (1)$$

where,

a_i = transfer function zeros

b_j = transfer function poles

k = proportionality constant

A problem occurs when one attempts to model a saturating system from its step response. The force sensor output resulting from a 7-volt step input is shown in Figure 18a, while that of a 2-volt step input is shown in Figure 18b. Figure 18a shows fast transient activity which saturates at

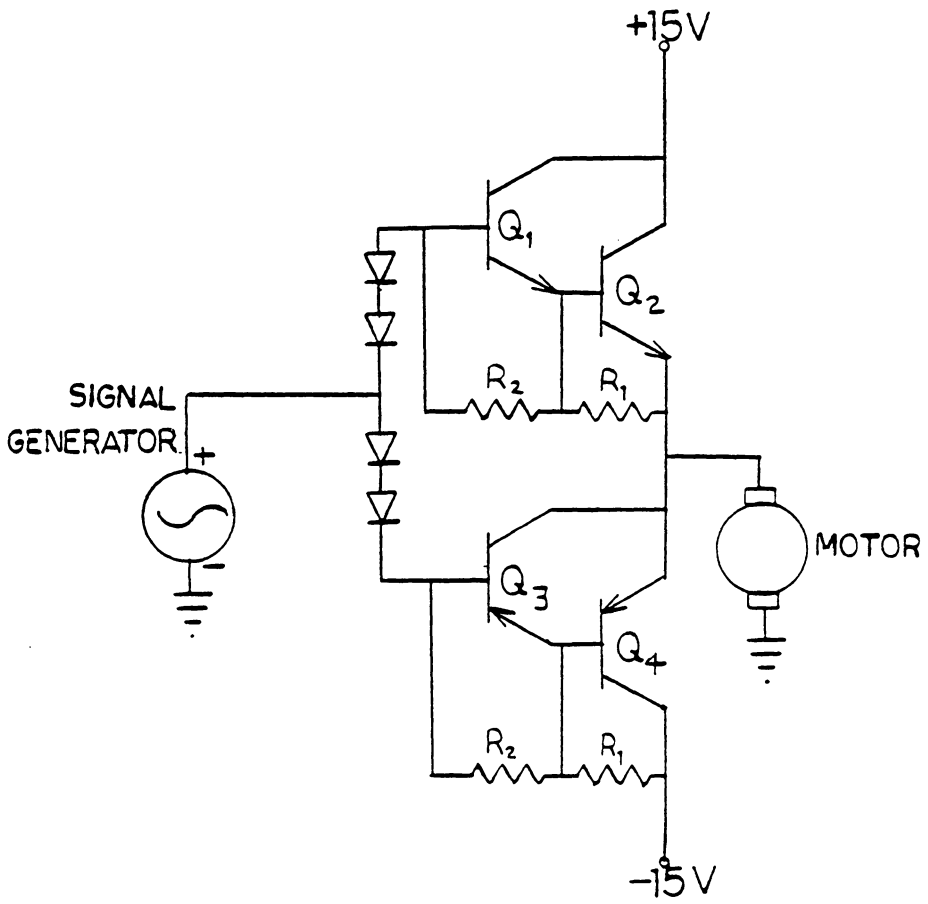

Figure 15. Continuous Power Amplifier

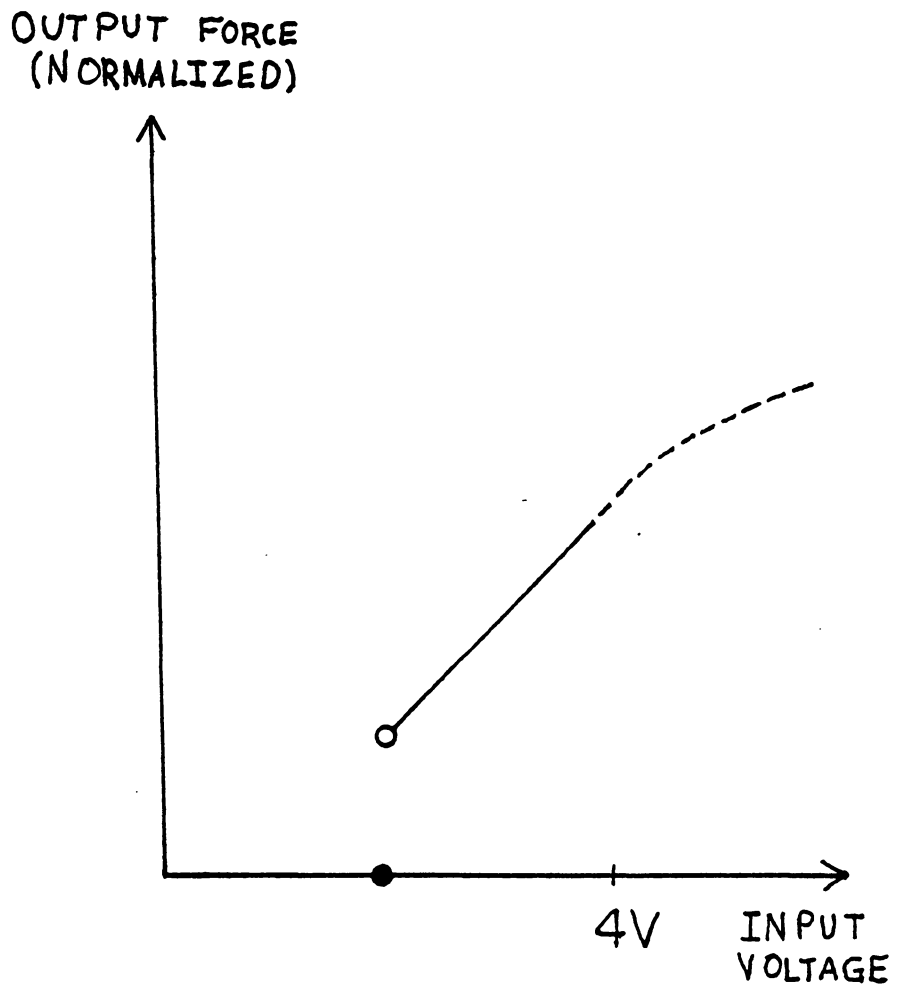

Figure 16. DC Response Using Continuous Amplifier

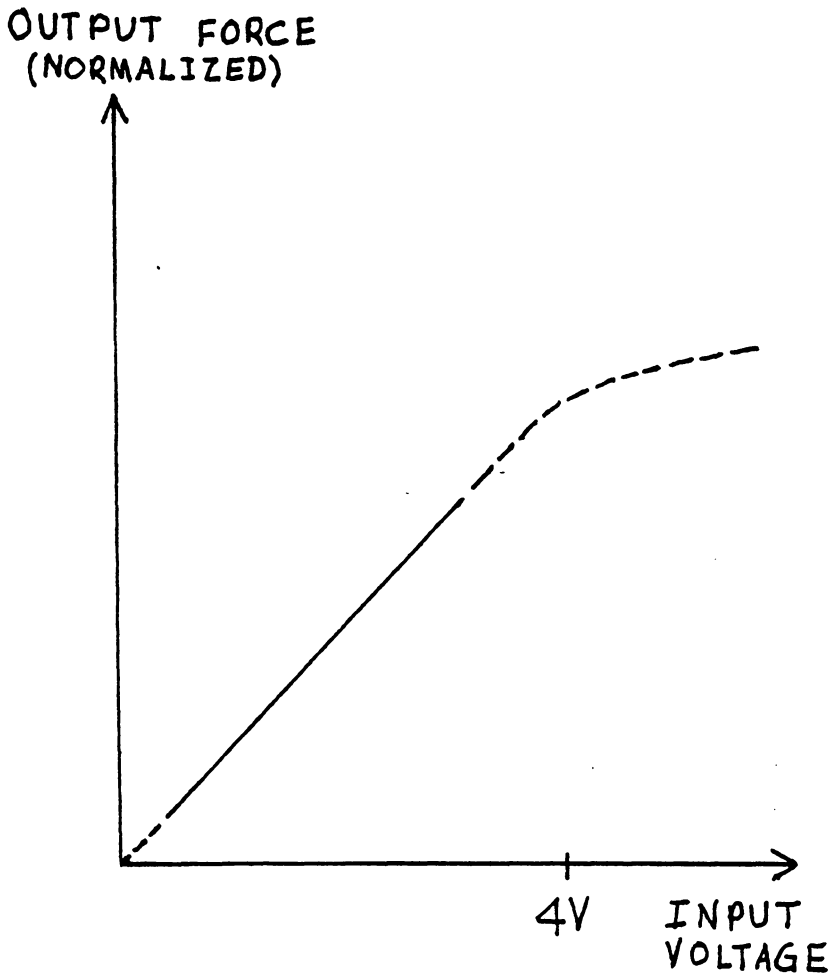

Figure 17. DC Response Using Bridge Amplifier

100mV in less than 2 seconds. Figure 18b rises almost linearly until it saturates at 30mV. The problem is to describe both of these step responses using a single transfer function. The solution is to use the step response shown in Figure 18a to model the fast dynamics, and assume the final flattening is replaced by a straight curve with positive slope. The justification for this simplification is as follows. A voltage step input is a velocity input for the motor. The motor maintains the desired velocity until the motor saturates. If the force is measured, and the input reduced to zero as the force approaches the desired value (as in a closed loop control system), and if the motor does not saturate before the input is reduced, the motor will not saturate. Therefore, since the system will operate at low levels of force, and small steady-state forces require no motor torque (as a result of gear box friction), this idealization is justified.

The model is constructed in a step-wise iterative process to approximate the dominant response while incorporating the above mentioned facts about the closed loop performance. First, the most important components of the response are modeled: the rise from zero to 50 millivolts, and the rise from 50 to 100 millivolts. These components are modelled as the sum of an exponential and an integral term as shown in Figures 19a and 19b.

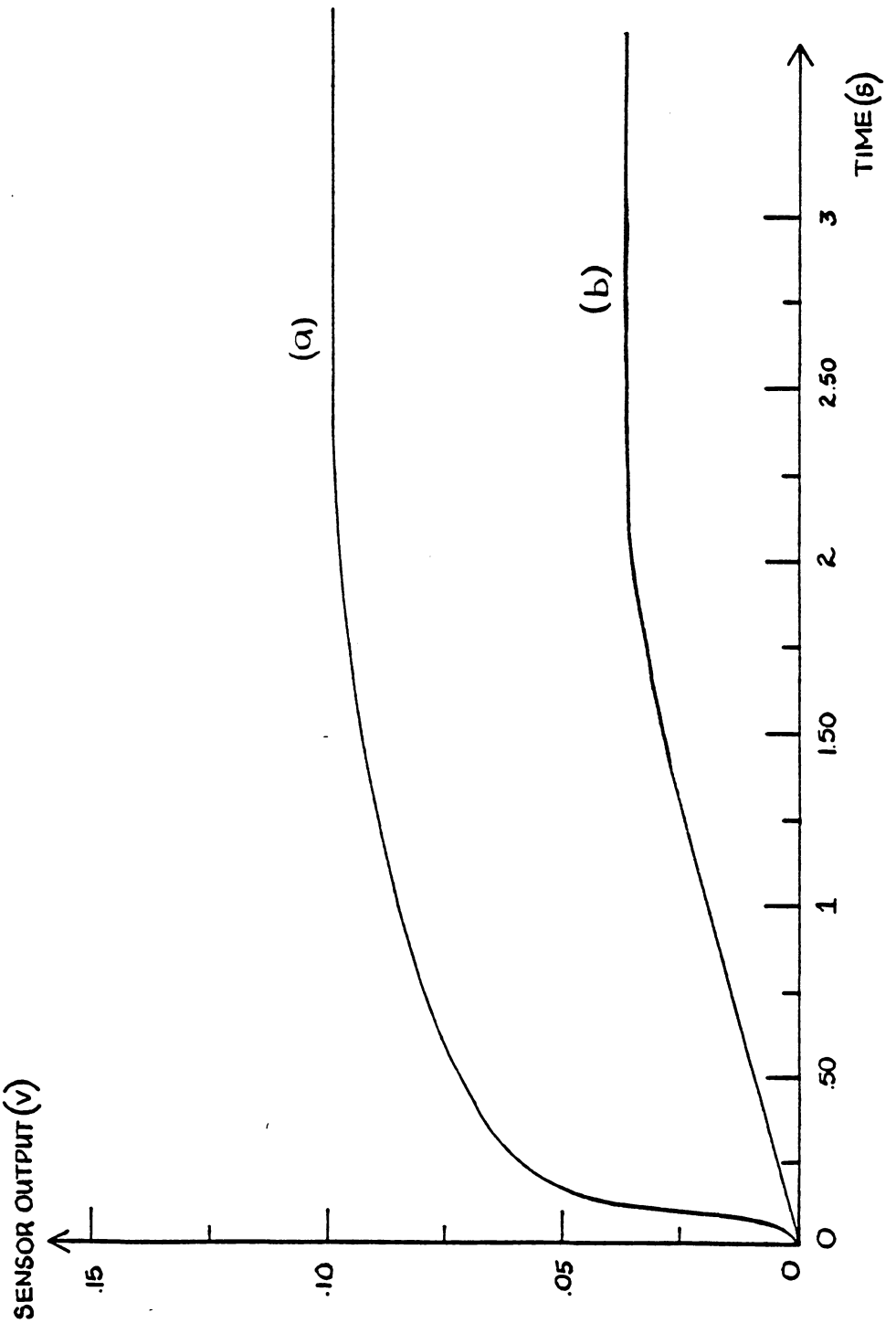

Figure 18. Experimental Open-Loop Step Responses

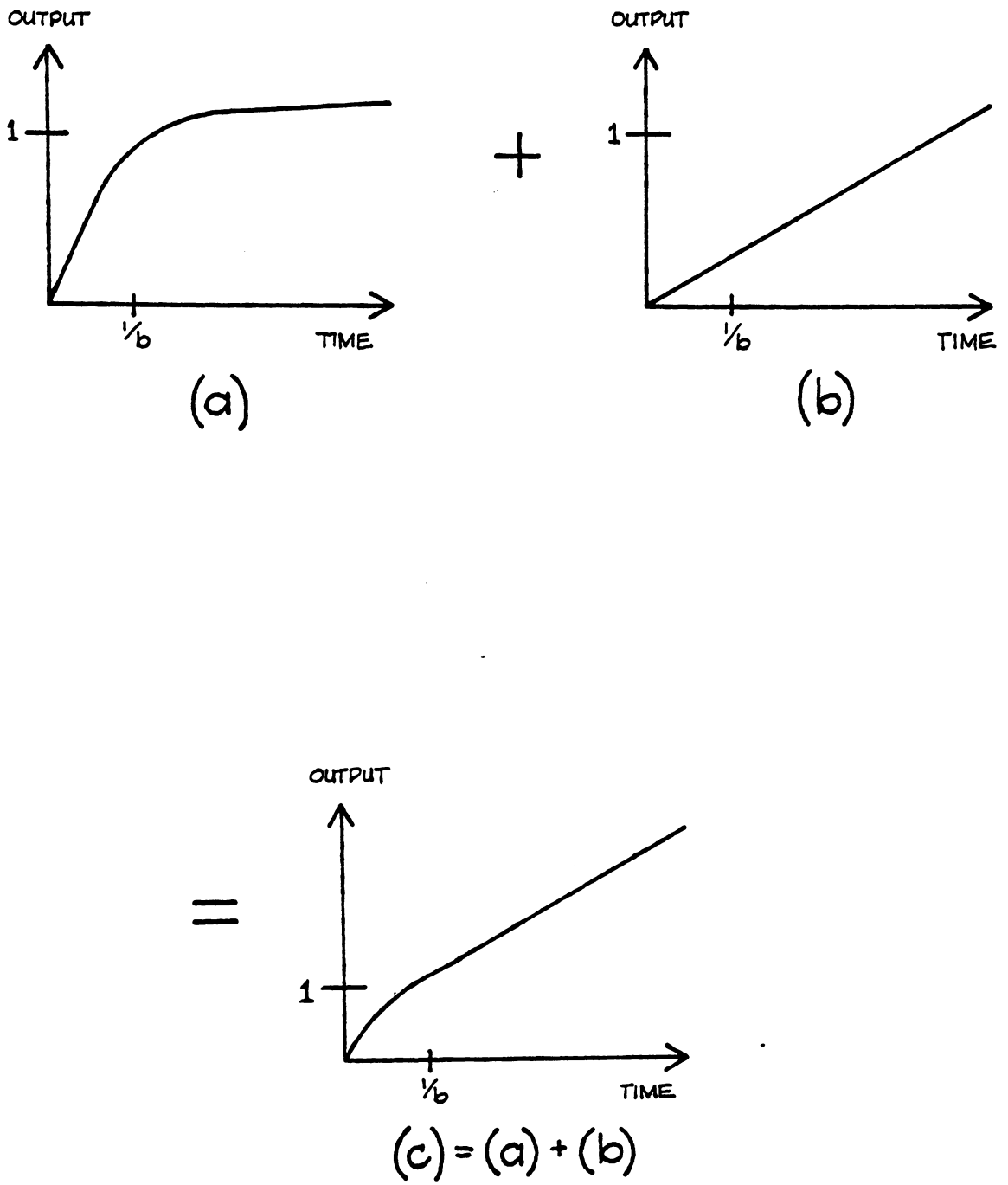

Figure 19. Components of the Model: a) exponential component, b)integral component, c) sum of exponential and integral components.

Figures 19a and 19b can be represented in the frequency domain as the sum of the Laplace transforms of each part. Multiplying by s to account for the step input yields the preliminary transfer function shown in (2).

$$G(s) = \frac{b_1}{(s+b_1)} + \frac{k_1}{s} = \frac{k(s+a_1)}{s(s+b_1)} \qquad (2)$$

The resulting response is shown in Figure 19c. This figure has nearly the same form as Figure 18a, but lacks the slight initial curvature and final flattening. The final flattening is ignored because no saturation occurs when the model is used, as was previously discussed. The initial curvature, however, is significant.

The model in (2) is not yet in the form required by (1). Since the numerator is first order, two additional poles must be chosen. One pole is found by iteratively matching the initial curvature to that of Figure 18a. The last pole is found using the Routh-Hurwitz stability criterion and the fact that the closed loop response becomes unstable when the feedforward gain K rises above 500. After scaling, the final transfer function is shown in (3).

$$G(s) = \frac{830\ (s+5.2)}{s(s+100)(s+50)(s+15)} \qquad (3)$$

A plot of the theoretical step response is shown in Figure 20. Note that the model given in (3) is already in its simplest form. No further simplifications are possible without sacrificing the ability to predict the relative stability of the closed loop system. Nonlinearities make higher order transfer function models meaningless.

3.2 RATE SENSOR IDENTIFICATION

The rate sensor, R(s), is also modelled from its step response, because no extremely wideband actuators are available for frequency response testing. As in the case of the open-loop system identification, some interpretation of the results is required. The step-response rise time of thin piezoelectrics is extremely small. The simplest available step-actuation technique of sufficient speed is the pencil-point-break technique first developed by Hsu to simulate a source of acoustic emission [12]. When a thin lead (0.5 mm) pencil point is broken, the force exerted by the lead drops to zero in less than a microsecond. Knowledge of the exact value of the input force is not essential because it will only have a scaling effect on the response. The most important part of the response is the initial rise, as will be shown.

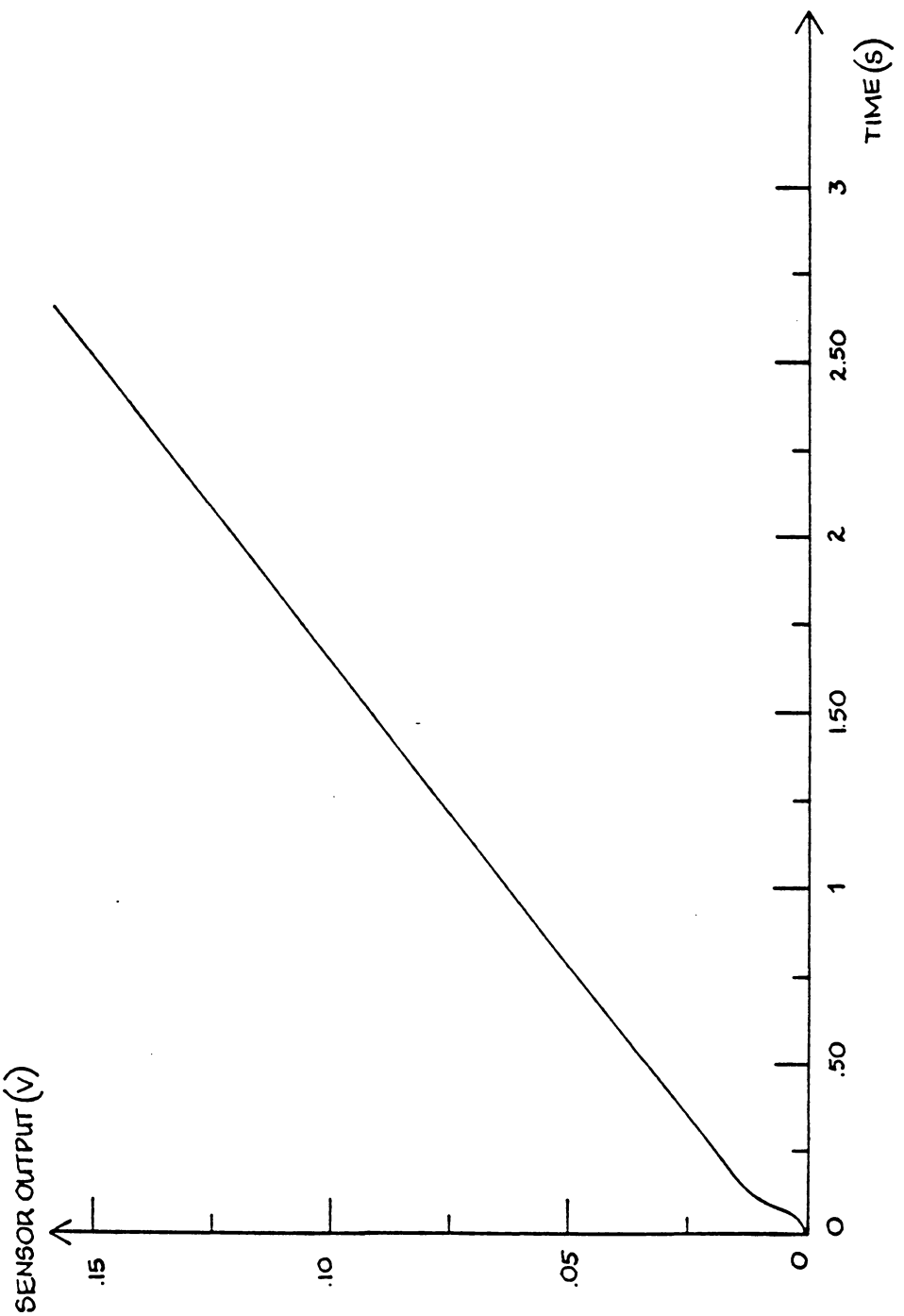

Figure 20. Calculated Open-Loop Step Response

The step response of the PVDF film across a 1 megohm resistor is shown in Figure 21. This response can be broken into two parts:

1) a 25 kHz high-frequency mode, and

2) a 2 kHz low-frequency mode.

To test for the source of the low frequency mode, the sensor was preloaded with weights before the pencil point was broken. Increasing the preloading reduced the low frequency mode, without affecting the high frequency mode. Thus, the low frequency mode is probably associated with oscillations of the surface after the unloading process. In the gripper system, the sensor will be used to sense impact forces and changes in force after contact is established. Therefore, the sensor will have some surface loading unless contact with the object is lost. Hence, the low frequency mode is ignored in the modelling procedure. The high-frequency response resembles the step response of a second order bandpass filter with an undamped natural frequency of 42×10^3 rad/sec, and a damping ratio of 0.3. Using these parameters, the transfer function (4) is derived.

$$R(s) = \frac{10^6 s}{s^2 + 1.4 \times 10^4 s + 1.8 \times 10^9} \qquad (4)$$

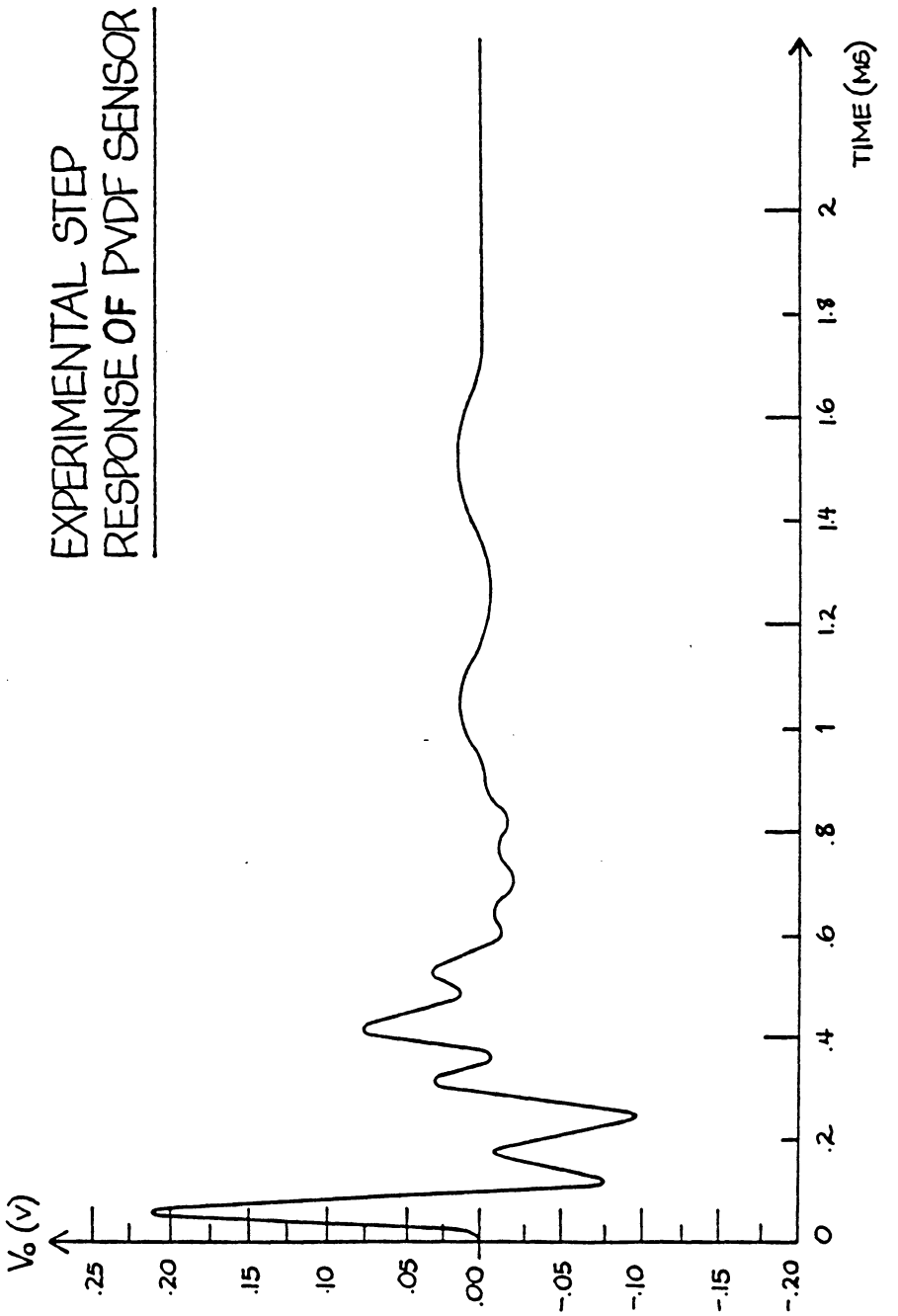

Figure 21. Experimental Step Response of the PVDF Sensor

The response of this filter is plotted in Figure 22. While this model does not fully represent all of the dynamics of the sensor, it is more accurate than an ideal differentiator.

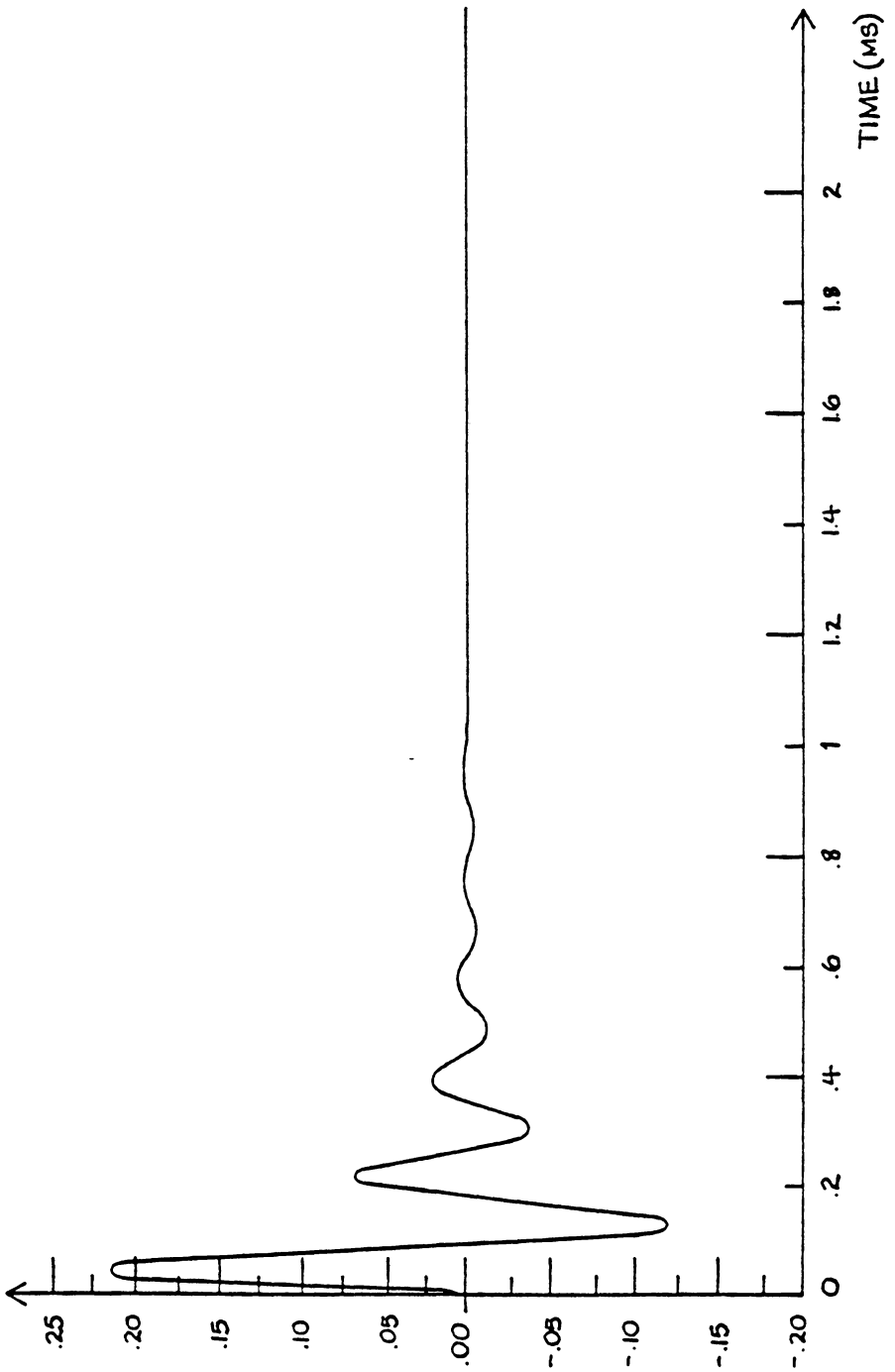

Figure 22. Calculated Step Response of the PVDF Sensor

CHAPTER IV. RESULTS

In this chapter, the results of tests which compare the closed-loop performance of the gripper with and without rate feedback are presented. Before the control system architecture shown in Figure 1 was selected, several others were considered. For example, the design shown in Figure 23 decouples the rate feedback and feedforward gains. This may have some advantages in certain applications, but in the selected design, overshoot is relatively insensitive to changes in the feedforward gain. If the feedforward gain is changed, the product of the feedforward and rate feedback gains will change in direct proportion. As a result, if the rate feedback is set to prevent overshoot at a particular feedforward gain, only small changes in the rate feedback gain will be required to continue the overshoot prevention for proportionately larger changes in the feedforward gain.

The results are divided into theoretical and experimental parts. In both parts, two basic tests are performed. The first test in each part demonstrates the ability of the additional feedback to prevent overshoot during a step transition in force. The second test compares the smallest achievable rise times with and without rate feedback. The description of the experimental results includes the results of an impact test using the PD control system.

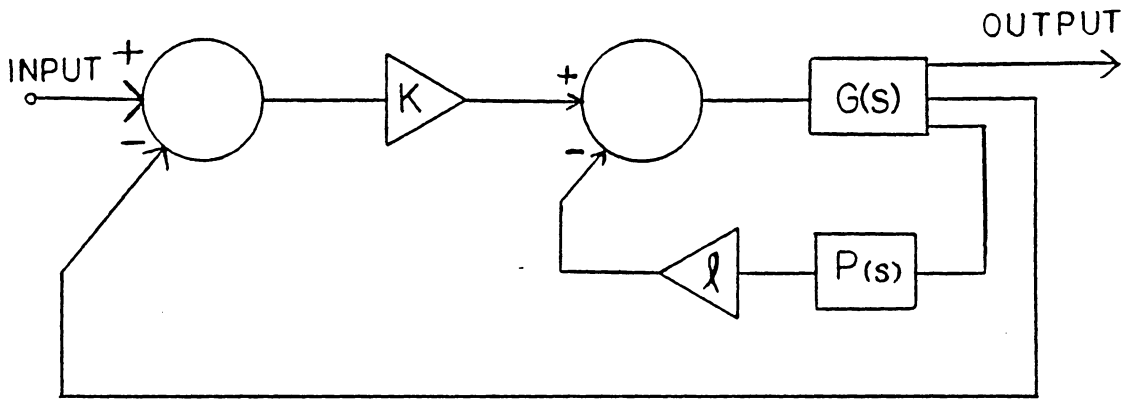

Figure 23. Alternate Control System Block Diagram

4.1 THEORETICAL RESULTS

In this part, step responses are calculated using the transfer function models constructed in chapter 3.

Test 1: This first test is designed to evaluate the ability of the PD control system to prevent overshoot during a step transition. The rate feedback gain ℓ is first set to zero. The feedforward gain K is raised to a value (300) which causes overshoot in the response as shown in Figure 24a. At this feedforward gain, the overshoot is 25 percent, and the settling time is 200 ms. If the feedforward gain K were increased further, the overshoot would grow larger, and the settling time would be longer. Next, without changing the feedforward gain K, the rate feedback gain is raised to a value (25) which reduces the overshoot to a smooth monotonic response as shown in Figure 24b.

The rise time in both cases is the same, but because oscillations about the steady state value are eliminated, the settling time is reduced to only 150 ms when rate feedback is included. Therefore, the models indicate that overshoot can be damped through rate feedback without sacrificing speed.

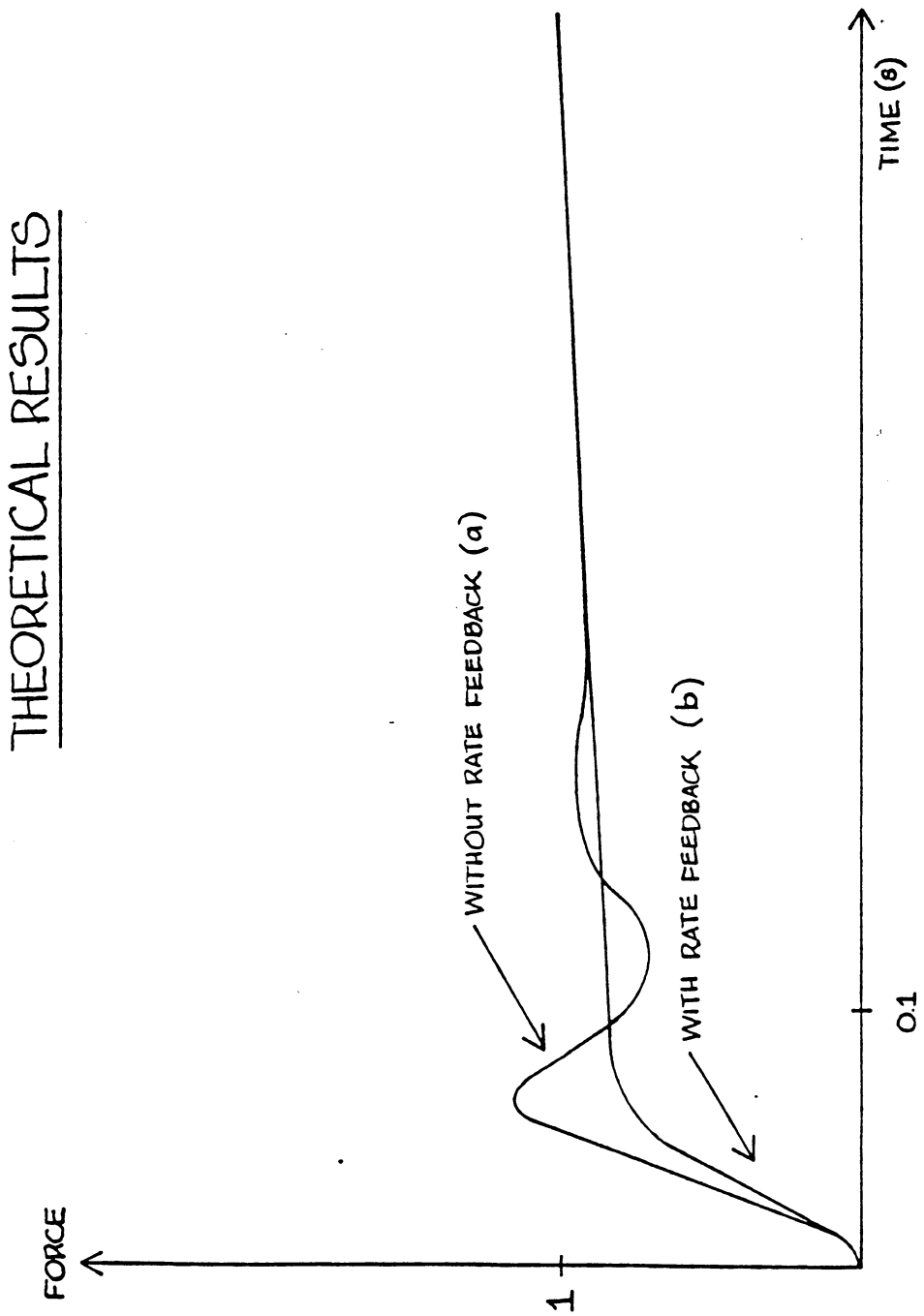

Figure 24. Theoretical Test of Overshoot Suppression: a) without rate feedback, b) with rate feedback

Test 2: This test demonstrates the response speed enhancement attainable using the PD control system. Since the PD control system allows the damping to be increased as the feedforward gain is increased, much higher feedforward gains may be used without overshoot. Figure 25a shows the step response of the proportional system (rate gain ℓ=0) when the feedforward gain is set such that the response is nearly unstable (K=500). The overshoot in force is 60 percent, and the settling time is 700 ms. If the rate feedback is raised to 30, all overshoot is eliminated, and the rise time is reduced to 60 ms as shown in Figure 25b. This is approximately the fastest rise time predicted by the models.

Higher feedforward gains require significantly higher rate feedback gains. These tend to overdamp the response to such an extent that longer rise times result. For purposes of comparison, Figure 25c is included to show the fastest rise time achievable without any rate feedback. Here the rise time is 500 ms. Figure 25c is actually the fastest monotonically increasing response without rate feedback. (The constraint of monotonicity is added to make the results more realistic. In the actual control system, if no rate feedback is used, all damping must come from friction. In practice, most non-monotonically increasing responses lead to actual overshoot due to backlash nonlinearities.) A comparison of responses in Figures 25b and 25c indicates that

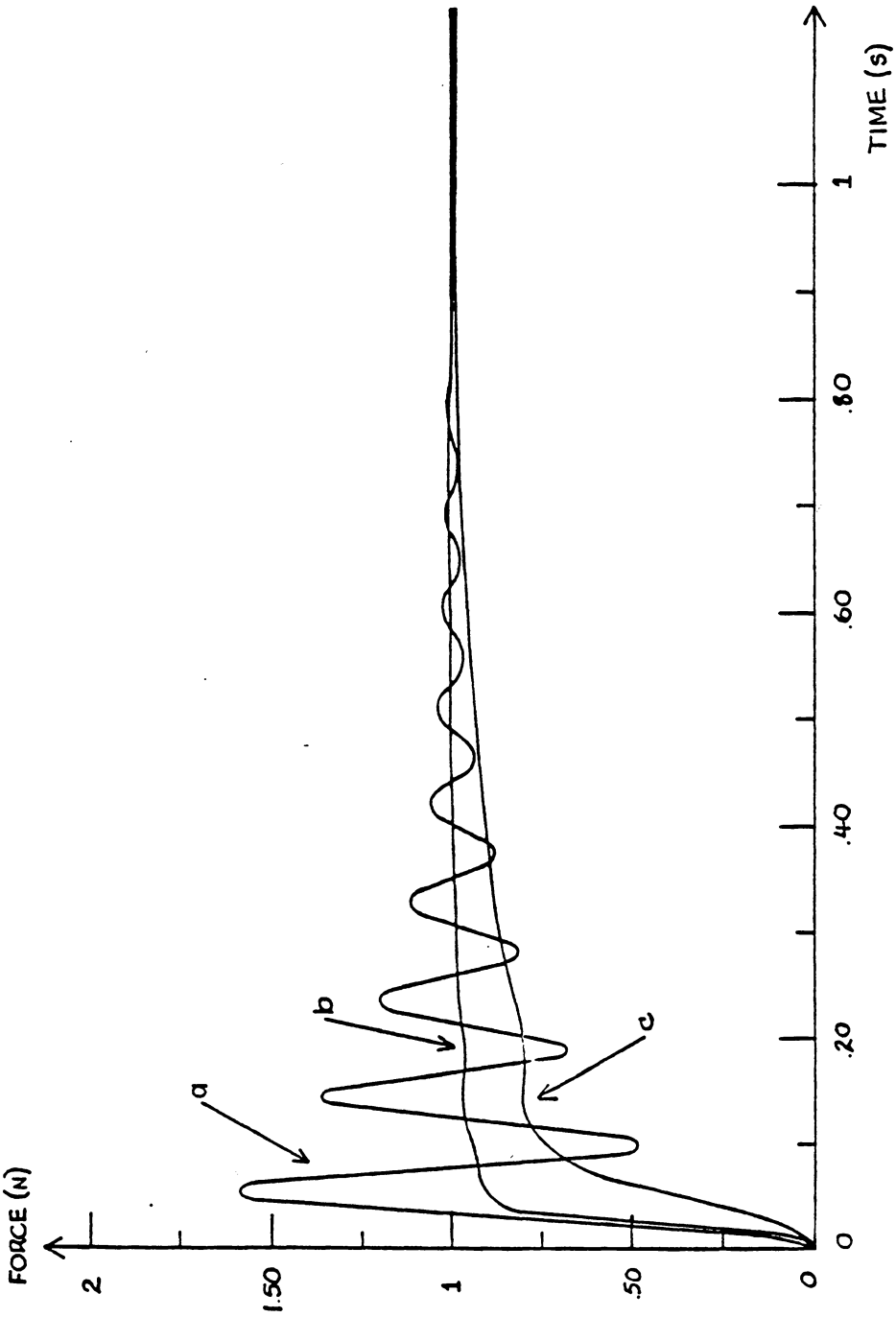

Figure 25. Theoretical Speed Enhancement: a) undamped response, b) damped response using rate feedback, c) damped response using friction.

an order-of-magnitude improvement in response speed may be possible.

Test 1 indicated that if the feedforward gain was held constant, the feedback gain could be adjusted independently to set the damping to a desired level. In fact, the damping can be set over a wide range, and can even be used to reduce the friction inherent in the gripper by changing the sign. The stabilizing effect of the rate feedback is clear upon examination of the root loci of the two systems. Figure 26 shows the superimposed root loci with and without rate feedback for the above two cases. The dominant poles move significantly closer to the right-half plane as the feedforward gain is raised from 300 to 500 in the proportional control system, while in the PD control system, the poles move away from the right half plane as the gain is raised.

This shows that the stability of the system can be increased with rate feedback. Also note that the damping ratio (ζ) of the dominant complex poles decreases sharply from $\zeta = .322$ to $\zeta = .213$ (a change of 40%) as the gain is increased in the proportional control system. However, it is only slightly decreased from $\zeta = .625$ to $\zeta = .608$ (a change of only 3%) in the PD control system. Thus, the damping in the proportional control system is more than 13 times more sensitive to a change in K than the PD control system.

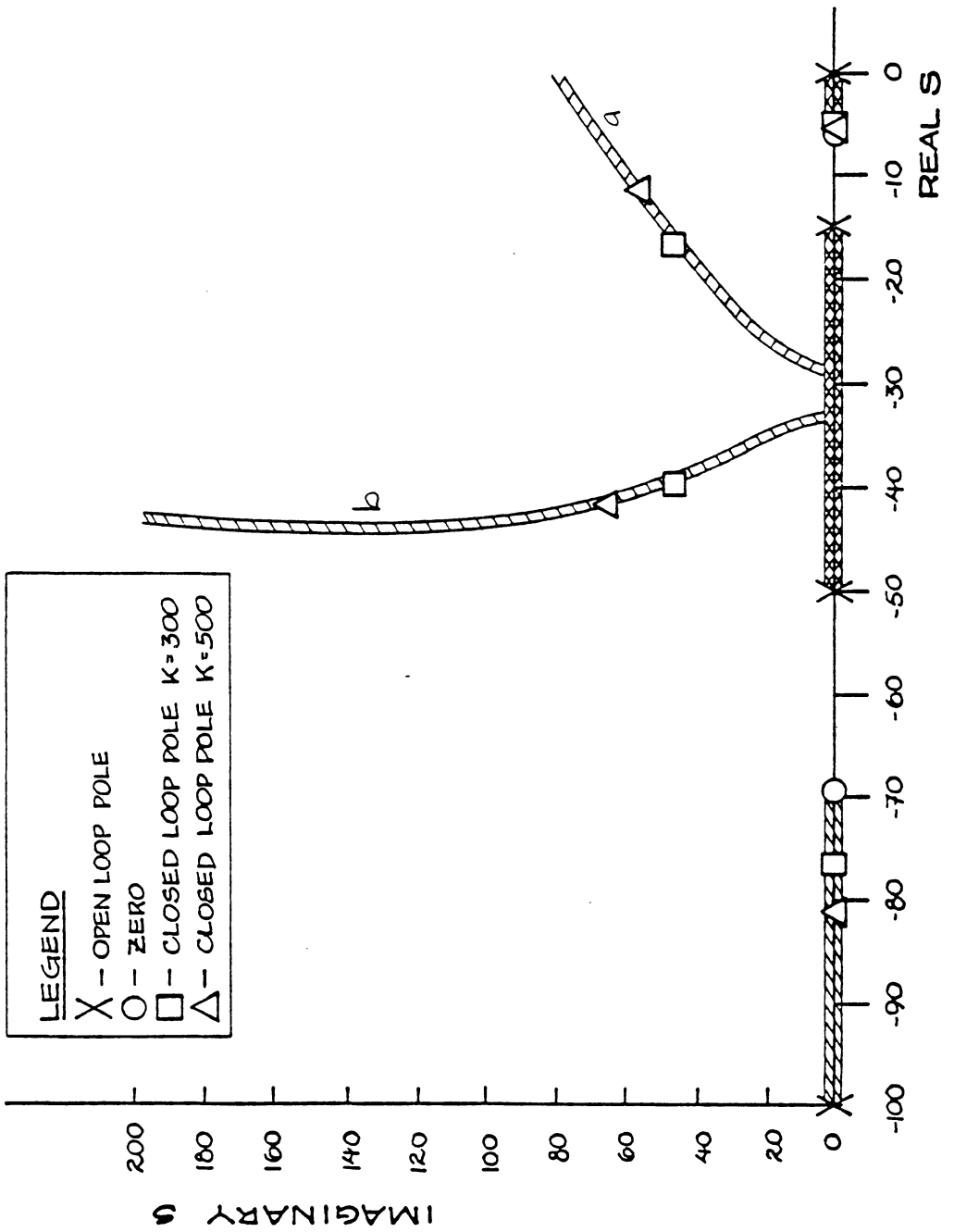

Figure 26. Root Loci: a) proportional control system, b) PD control system.

4.2 EXPERIMENTAL RESULTS

The theoretical results reported above were experimentally tested using the hardware described in Chapter 2. The output force was detected by the feedback force sensor and recorded on a digital oscilloscope, and the results presented are plotted from the oscilloscope.

Test 1: Figure 27a shows the step response when the feedforward gain is adjusted to respond with a moderate amount of overshoot, as in the first theoretical test without rate feedback. The response shows larger oscillations than were present in the calculated response, but the rise time and settling time are roughly the same. The oscillation discrepancy between the calculated and experimental responses is probably caused by frictional effects which are not included in the model of the gripper.

When rate feedback is included (same feedforward gain), the overshoot is completely suppressed, as shown in Figure 27b. As in the theoretical response, the rise time is virtually unaffected by the additional feedback, and the settling time is reduced.

Test 2: In this part, the maximum response speed with and without rate feedback was experimentally measured. First, the most rapid response without rate feedback was determined

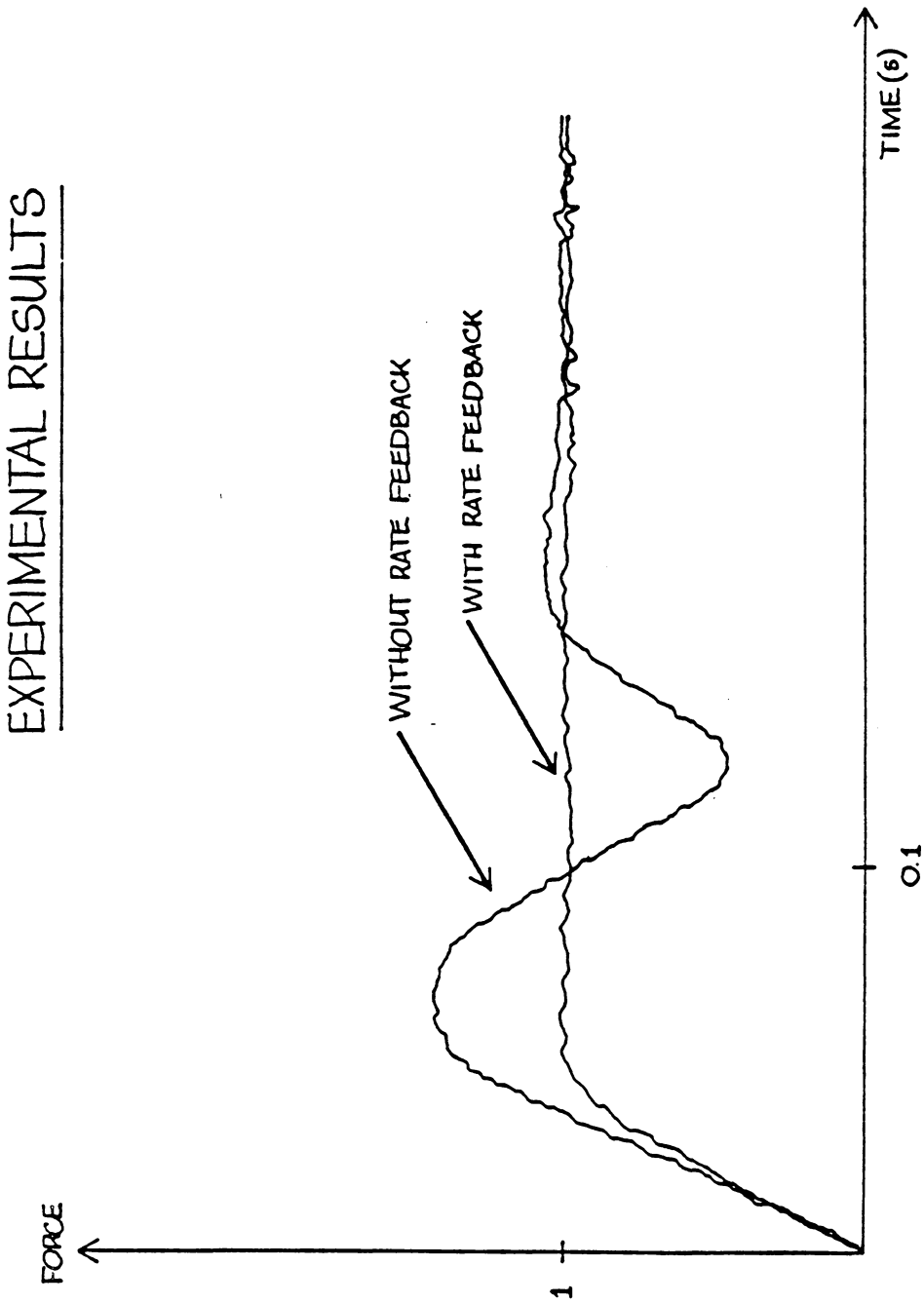

Figure 27. Experimental Overshoot Prevention Test: a) without rate feedback, b) with rate feedback.

by the criteria outlined above in test 2 of the theoretical results. This response is shown in Figure 28b to have a rise time of 2 seconds.

Next, the feedforward gain and rate feedback gain are increased together to achieve the minimum step response rise time of 90 ms as shown in Figure 28a. Thus, the results of the experiment indicates that the response time can be improved by more than an order of magnitude using rate feedback.

Impact Test: This section closes with a nonlinear experiment which extends the previous experimental results to real life gripping conditions. In the previous tests, the gripper was always in contact with the object, with some small initial contact force. In the actual gripping processes, however, the gripper would usually close unimpeded until it made contact with the object to be grasped. Figure 29a shows the step response when the wide-open gripper closes with proportional feedback onto an object placed symmetrically between its fingers. The initial part of the response is zero because no contact exists as the gripper closes. Then the response jumps to more than 300 percent of desired value, rebounds, breaks contact with the object, and impacts again. The second impact is at lower initial velocity, and the response is damped by friction after 2 seconds. The response finally reaches steady state (not shown) after 10 seconds.

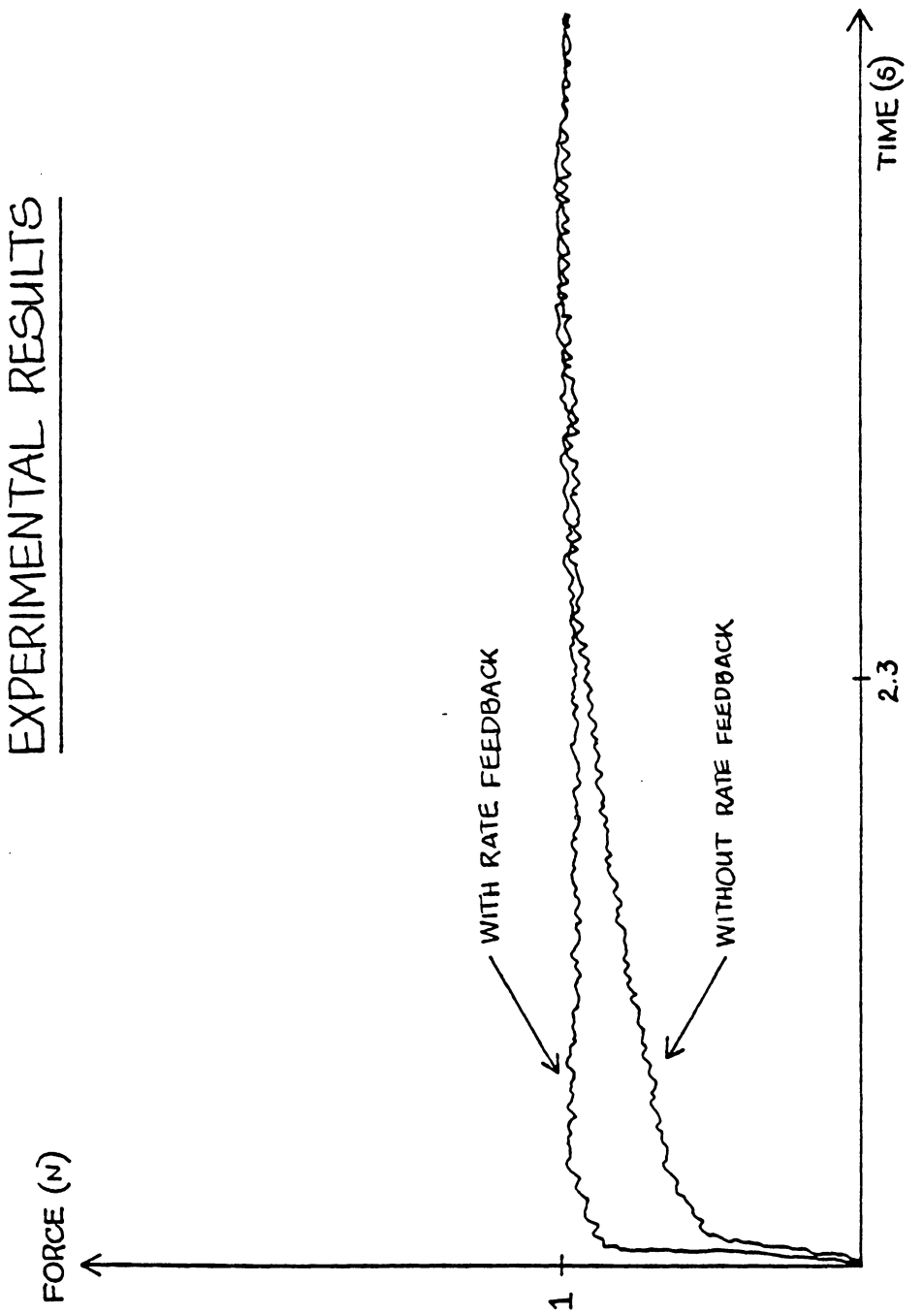

Figure 28. Experimental Test of Speed Enhancement: a) response with feedforward and feedback gains adjusted simultaneously, b) best response without rate feedback.

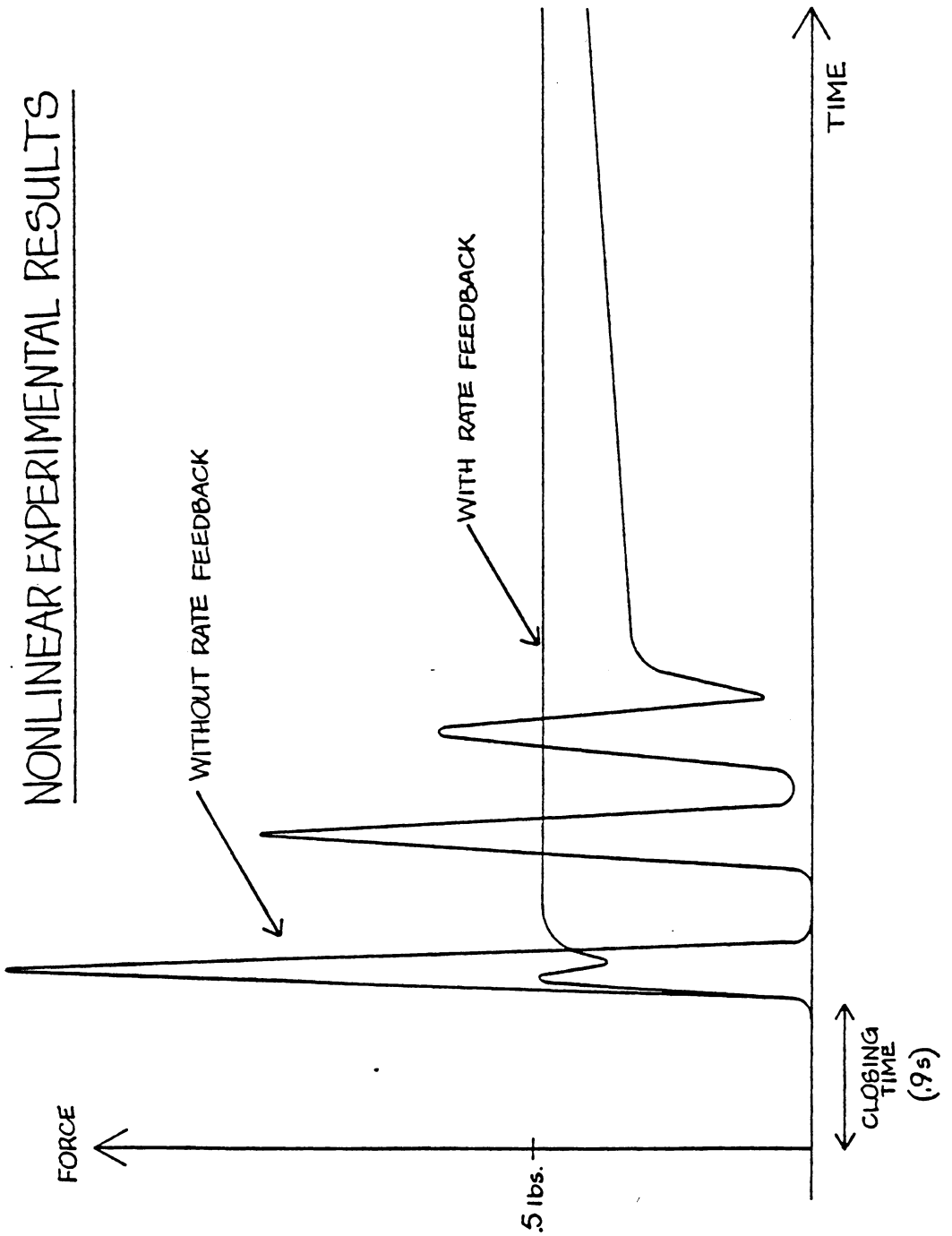

Figure 29. Experimental Impact Test: a) step response without rate feedback, b) with rate feedback.

In contrast, Figure 29b shows the step response when the system is adjusted with the same feedforward gain as above, but rate feedback is included. This response exhibits only a few percent overshoot, and the settling time is 300 ms (after impact). Thus, the rate feedback should provide significant improvement in the performance under practical gripping conditions.

CHAPTER V. FUTURE RESEARCH

The purpose of this investigation has been to analyze the quantitative benefits of using the PVDF sensor in a PD servomechanism for controlling a particular gripper. The results presented indicate that significant benefits can be obtained under certain conditions. In this chapter, two broad (and somewhat interrelated) areas of further research are discussed. First, more specialized problems are discussed which relate to the Rhino robot, or some other particular gripper. The specialized problems are in open-loop system modelling, development of control laws, and in electronic design. Secondly, more general problems are discussed which relate the results obtained here to more general problems in gripper control. These include the design of hierarchial control algorithms which integrate the sensors described in this paper into the overall sensor system of the robot, and in further sensor characterization and design.

5.1 SPECIALIZED RESEARCH

In Chapter 3, it was shown that a linear model for the open-loop system could be developed despite the presence of significant nonlinearities in the system. A more specialized

inquiry into the characteristics of the system should start with improving the modelling technique. First, the present model could be improved using a sensitivity analysis in conjunction with experimental simulation. If sensitivity functions were computed and plotted in time for each of the closed-loop pole locations, then the differences between the experimental and theoretical step responses could be minimized in a structured manner. This should provide some initial improvement over the model presented, which was identified largely by trial and error. This would lead to a better linear model, but backlash nonlinearities would undoubtedly have to be included explicitly in the model.

In addition to avoiding the backlash nonlinearity, the modelling procedure required that forces be limited to low levels to avoid saturation nonlinearities in the motor. For low levels of force, the system can operate linearly under closed-loop control. As the torque exerted by the motor increases, the saturation nonlinearity becomes significant. The small-signal constraint could be lifted, however, by using a torque-dependent compensator. The torque could be easily sensed by measuring the current drawn by the motor. Such a compensator would allow linear operation to be maintained until the onset of motor saturation.

Once these theoretical and practical changes are made, it should be possible to accurately simulate the response over the entire range of gripping forces. Then two experiments

would be in order: a more thorough comparative investigation of the usefulness of the rate feedback sensor, and an investigation into the development of more complex control laws. The complexity of these experiments requires flexibility in the electronic devices used to implement the control. Serious consideration should be given to abandoning analog circuitry and using a more flexible digital controller.

5.2 GENERAL RESEARCH

5.2.1 SYSTEM INTEGRATION

Another test of the effectiveness of the rate feedback technique is to test the system performance when additional sensors are used in conjunction with the touch force sensors. In this thesis, the gripper control is based on the feedback from the force and rate-of-force sensors. Usually, other variables such as position are available for control. In this section, generalization of the results to a multisensor system are considered. Three types of sensors are currently under development. They are high-precision position sensors [1], ultrasonic or optical proximity sensors [7], and array-force sensors [3]. Figure 30 shows a parallel-jaw gripper similar to the Rhino robot gripper described in Chapter 2.

The gripper is instrumented with integrated force and rate-of-force sensors, tactile image sensors, an ultrasonic ranging sensor, and a position sensor for sensing the distance between the jaws of the gripper. In addition, the gripper is mounted on a drivable mount which adds an extra degree of freedom (additional degrees of freedom could be included similarly). The mount has a sensor to measure the position of the gripper relative to the manipulator arm. The ultrasonic or optical sensor would aid positioning the gripper around the object, but would not play a direct role in the feedback control system. A control system utilizing the dynamic sensors is shown in Figure 31. (Note: the tactile image sensors are not considered dynamic.) This control system would be supervised by a computer which would use the data from all of the sensors (including the tactile image sensors) to change the position inputs, force inputs, and control gains. The computer might set the gains using a heirarchial scheme which would depend on stiffness and damping requirements. As the PVDF sensor becomes more deeply embedded in the system, its margin of improvement may either increase or diminish. The results of such analysis may strongly influence the design of future robot sensor systems.

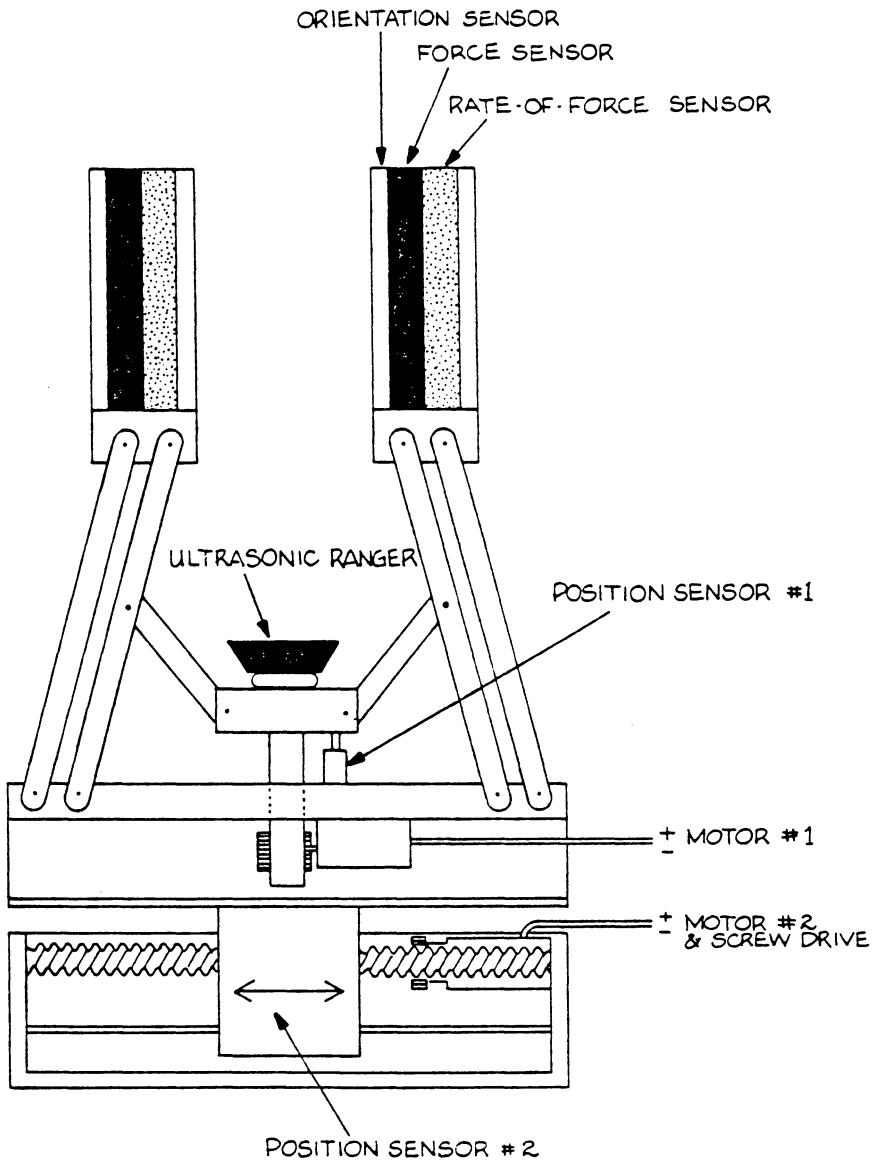

Figure 30. Instrumented Gripper: a) Force Sensors, b) Rate-of-Force Sensors, c) Position sensors, d) Ranging Sensor.

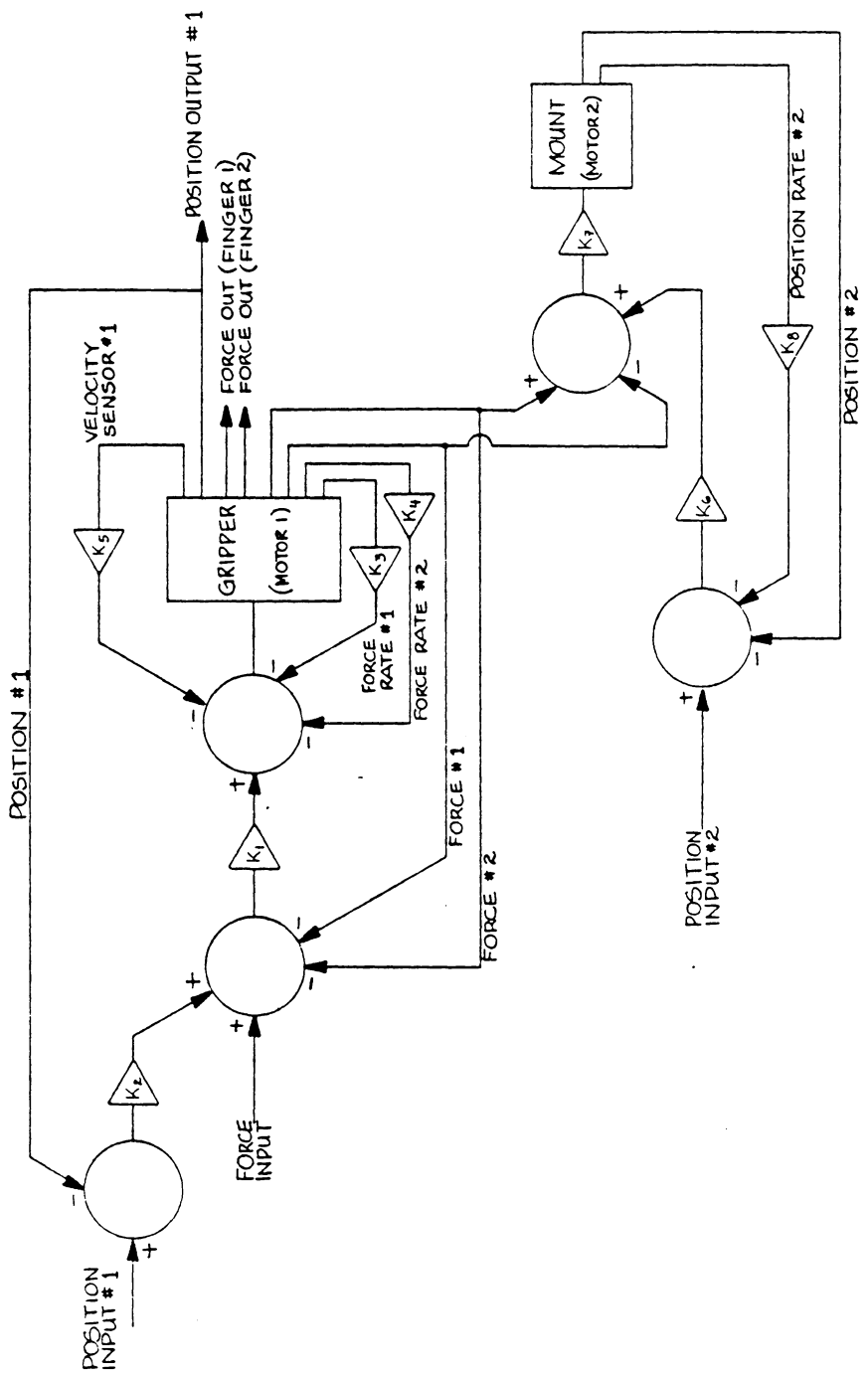

Figure 31. Control Block Diagram

5.2.2 SENSOR RESEARCH

Any further developments in sensor technology could affect all gripper controllers, and are therefore a topic of general future research. Many avenues of continued research exist in sensor technology. First, better sensor modelling is essential for further improving the accuracy of simulations. Sensor modelling will require superior testing procedures, and a serious inquiry into the physics of the response. In addition to modelling, utilization of tangential force detection poses challenging problems. Finally, improvements in sensor construction methods are important.

In Chapter 3, the rate sensor was modelled by a pencil-point-break test. In a linear system, a step unloading should be identical to an inverted step loading. In the case of the pencil point break test, however, the fact that the force is reduced to zero excites surface oscillations which constitute a form of nonlinearity. Presumably, these surface oscillations should be significantly damped in a step loading, but the differences between step loading and unloading deserve close inspection. Furthermore, the effects of other assumptions such as the force distribution should be analyzed. For instance, the force is assumed to be evenly distributed on the sensor as the force is applied. This is obviously not the case for this test procedure. The pencil point is small relative to the size of the active area of the

sensor. The effects of these approximations require close analysis which could become extremely involved.

Throughout this paper, only the normal response of the PVDF sensor has been considered. However, the film can be polarized so that it is sensitive to shear forces as well as normal forces. A PVDF sensor which can sense shear forces could be used to control the rate at which an object slips in the grip. The response of such a sensor could be included in the hierarchial control system discussed in 5.2.1. The shear response is generally much greater than the normal response. If normal forces are converted to shear stresses, the signal-to-noise ratio could be improved tenfold. Stochastic models which include the effects of noise might be developed to analyze the implications of such an improvement in the signal to noise ratio.

Finally, the sensor construction could be improved. For instance, it is not necessary to cast the sensor to make the connection. Alternatively, a partial poling technique [5] could be used to allow piezoelectrically-insensitive metallic tracks to make the connections. The backing material might also play a significant role in the performance of the sensor. An analysis into the the effects of the backing material should yeild an optimal choice of materials, and their thicknesses.

CHAPTER VI. CONCLUSION

A robot gripper control system has been constructed and analyzed to evaluate the usefulness of piezoelectric rate-of-force sensor feedback in gripper force control. Rate sensing was shown to provide a method of actively damping the force exerted by the gripper. Specifically, the rate feedback was shown to be effective in suppressing overshoot occurring during step transitions in force, and in improving the step response settling time by as much as an order of magnitude. Other test results were shown to demonstrate the possible extensibility of this technique to the damping of impact forces. Overall, this investigation indicates that significant advantages result from the use of piezoelectric rate-of-force sensors in the control of robot grippers. The ultimate usefulness of this technique awaits the evaluation of its benefits when adapted to practical gripping applications.

APPENDIX: PVDF SENSOR CONSTRUCTION

The construction of the PVDF piezoelectric sensor was briefly described in Chapter 2. In this appendix, a detailed "recipe" for building the sensor is given. The technique is an inexpensive adaptation of the design developed by Dario et al [6]. Extension of the construction technique to multielement sensor design is also discussed. The presentation is broken into eight simple steps.

1. Purchase Film

The two major manufacturers of PVDF film are Pennwalt Corp.[2] in USA, and Solef[3] in Belgium. The product by Solef has the advantage that it is sensitive in two orthogonal stretch modes, as well as in the normal mode. The product

---

[2]

KYNAR Piezo Group
Pennwalt Corporation

P. O. Box C
King of Prussia, PA 19406-0018
Tel.

[3]

Dr. J. P. Bex
Soltex Polymer Corporation

Houston, TX 77098
P. O. Box 27328
Houston, TX 77027
Tel.

from Pennwalt (in 1985) is sensitive in only one direction of stretch. The film is also made non-commercially at several research laboratories such as the National Bureau of Standards (NBS), in Gaithersburg, Maryland.

This application only requires sensitivity to normal forces, as was discussed in Chapter 2. Therefore, the film from Pennwalt is adequate. Two square inches of film is enough to build several sensors (or cover for a few mistakes). The film thickness selection is a matter of compromise. The thin film (less than 20 microns) offers wider bandwidth and higher capacitance, while the thick film (more 50 microns) has a stronger piezoelectric response, is less susceptible to interference, is somewhat easier to work, and is usually manufacured with thicker surface metalization. (The piezo film is a transparent dielectric, but is manufactured and sold with a conductive coating (either aluminum, nickel, or tin) on both sides. Some piezoelectrics such as quartz and Rochelle salts are spontaneously piezoelectric. Other piezoelectrics such as barium titanate and PZT must be polarized in the presence of a strong electric field. PVDF is a piezoelectric of the second type in that it must be polarized. The conductor deposited on the film is required to evenly distribute the electric field during the poling process.) The practical considerations and the strong re-

sponse make the thicker film the preferred choice. The 52 micron thickness was chosen for the transducer used in this project.

2. Cut the Film

The film is delivered in sheets which must be cut to the desired size. The film can be cut using either a sharp knife (such as an X-acto blade), or using scissors. Scissors work best, but continuity between the top and bottom surfaces should be checked afterword to avoid the effects ofaccidental connection between conducting surfaces. The film used to build the transducer described in the text was cut into a square with 1.5 cm sides.

3. Resist

The transducer is sensitive anywhere the film is covered on both sides by conductor metalization. Removing conductor on either side removes the sensitivity in that area. It is advantageous to leave the entire front surface clad for electro-magnetic interference protection. The front surface in therefore necessarily equipotential, and serves as the ground reference. On the backside, all conductor should be removed except where sensitivity is desired. The technique presented here can be used to create multielement arrays, as

well as single element sensors. Experience indicates that 4x4 arrays with 2 mm separation can be built using this technique. Larger arrays, or arrays of higher density must be built using a more sophisticated (and expensive) technique. The conductor will be removed in an acid bath, but first resist must be applied to prevent the acid from removing all of the conductor. Simple resists such as tape and nail polish can be effective, but the most effective resist is printed circuit ink. (Printed circuit ink is designed for use in a silk screening process. A good printing circuit ink is ER-6055A Blue manufactured by the Colonial Printing Ink Company, East Rutherford, NJ 07073. Silk screening is necessary for etching complex patterns such as those required for the construction of array sensors, but is not necessary for single element transducers.) To build a single element transducer, clean the metallic sufaces with freon and coat all of one side of the film with resist, except for a small area at one of the corners. The corner which is not covered with resist will be used to indicate when the etching process is complete. Let the side dry at least four hours at room temperature. Next, on the other side, apply resist in a circular spot in the center of the film. The size of the spot will determine the size of the sensitive area. Let the resist dry overnight.

4. Etch

Remove the desired metalization by etching with concentrated hydrochloric acid (HCl). Place the film in a 500 ml glass beaker. Wear plastic gloves and goggles, and work under a fume hood. Add about 50 ml of the concentrated HCl to the beaker, and gently agitate the beaker until the indicator corner is clear of metalization. Usually, the film can be etched in less than one minute, but the etching time depends on the concentration of the HCl, and the thickness of the metalization. After etching, rinse the film and the beaker with clean water and allow the film to dry. After the film has dried, remove the resist with turpentine to expose the metallized pattern and ground plane.

5. The Mold

The mold was built from plexiglass, and lined with mylar for easy removal. Cut the pieces in Figure 32 from half inch plexiglass, sand the sawed edges smooth, and drill the holes. Glue the small front piece (shown with no screw holes in Figure 32) in place on the base. The casting process requires two pourings. This short piece will be the level of the first pouring. Wrap each of the pieces of plexiglass with mylar. Mylar is a type of sheet plastic which is most readily available through camping stores where emergency blanket made of mylar are sold. One side of the emergency

blanket is metalized. The metalized side should not be exposed in the mold. Before wrapping the base, apply some petroleum jelly to the surface to assure even contact. Screw the assembly together and proceed to the next step.

6. Lead Attachment

The inner conductor of a small-diameter coaxial cable is attached to the etched-out spot on the backside of the film, and the outer conductor is attached to the front surface as shown in Figure 3b. First, carefully bend a 0.3 cm crease along one side of the film as shown in Figure 3b. (Variation: Cut 0.3 cm sq. corners from the film, and crease all four sides.) The crease(s) perform the double function of providing a means of grounding the front surface, and preventing the film from lifting at the edges. The leads cannot be soldered to the PVDF using ordinary electronic grade solder because the film would melt. The leads could be attached using special low temperature solder, but the simplest technique is to use a conductive epoxy such as the E-solder manufactured by Acme Chemicals and Insulation Company, New Haven, CT. E-solder is a silver-filled epoxy adhesive which exhibits high conductivity when correctly prepared and cured. Remove about 1.5 cm of the outer insulation from the coax. Pull back the braided outer conductor, and twist the braid into a single strand. Remove 0.3 cm of the inner insulation,

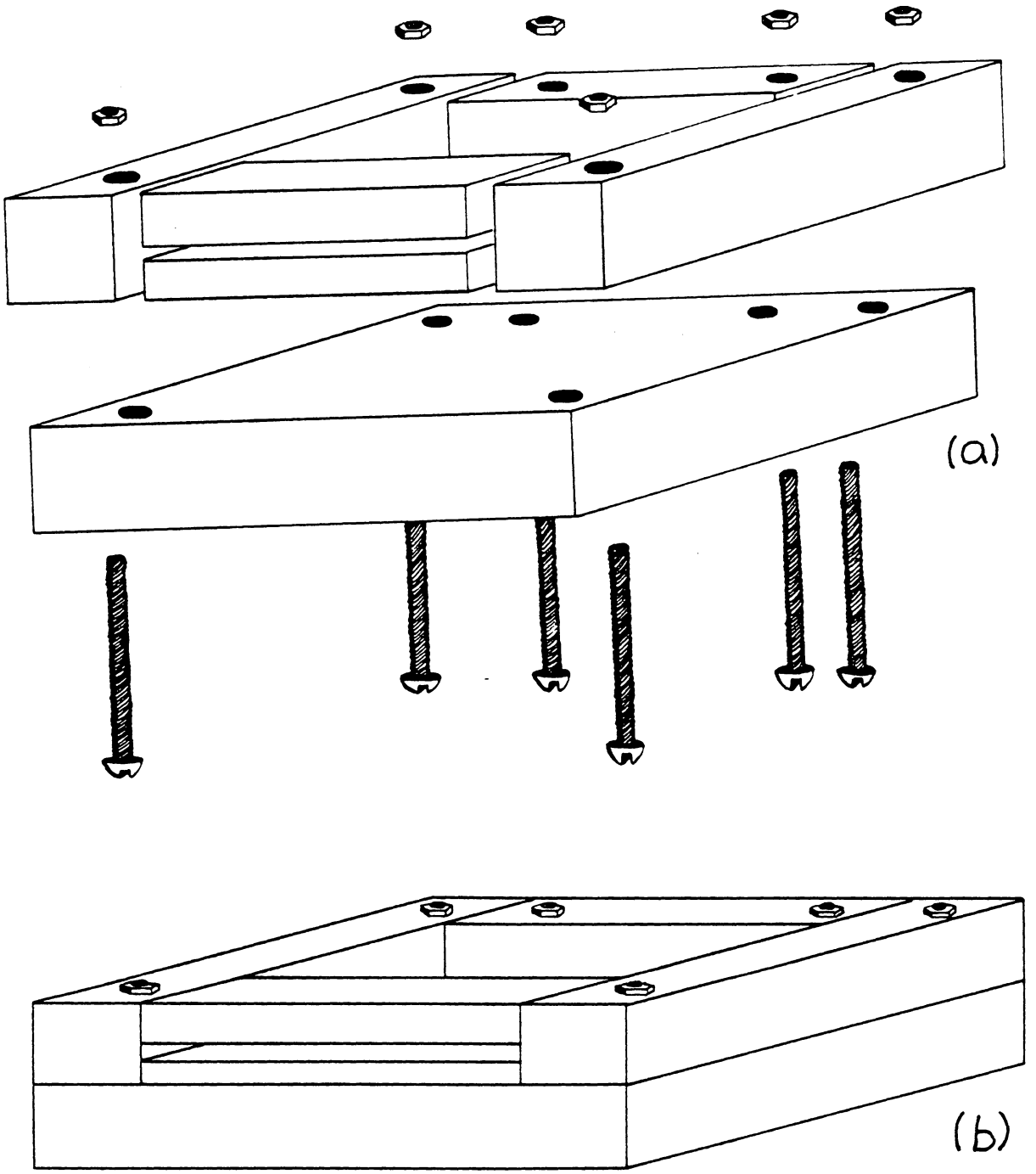

Figure 32. Mold for Casting the Sensor: a) Exploded View, b) Assembled View.

and twist the inner conductor into the shape shown in Figure 33a. Prepare the silver epoxy according to the directions on the package. Be sure to mix the epoxy for several minutes before glueing the wire to the film. Bend the wire so that it can rest in position, as shown in Figure 33b. Glue the leads to the film. Place the film under a light bulb to warm the glue to about 70 degrees Celsius.

7. Cast

The casting process encases all but the front surface of the film in an epoxy block. This epoxy provides both a means of concentrating forces in a normal direction against the sensor, and a means of supporting the connecting cable (or cables in the case of array sensors). Remove the top half from the split side of the mold. Tape the front surface of the film down in the middle of the mold using two-sided tape. The folded-up edges should not be taped to the mold because they should be encased in the casting. Using needle-nose pliers, hold the cable 2 mm above the connection, and bend the coaxial cable toward the split side of the mold. Place a wad of plastic wrap over the cable as a seal, and replace the top half of the split side. Now the sensor is ready to be cast in a single pouring. As an alternate procedure (particularly useful when constructing array sensors), do not bend the cable until a 2 mm high cast has been formed. After

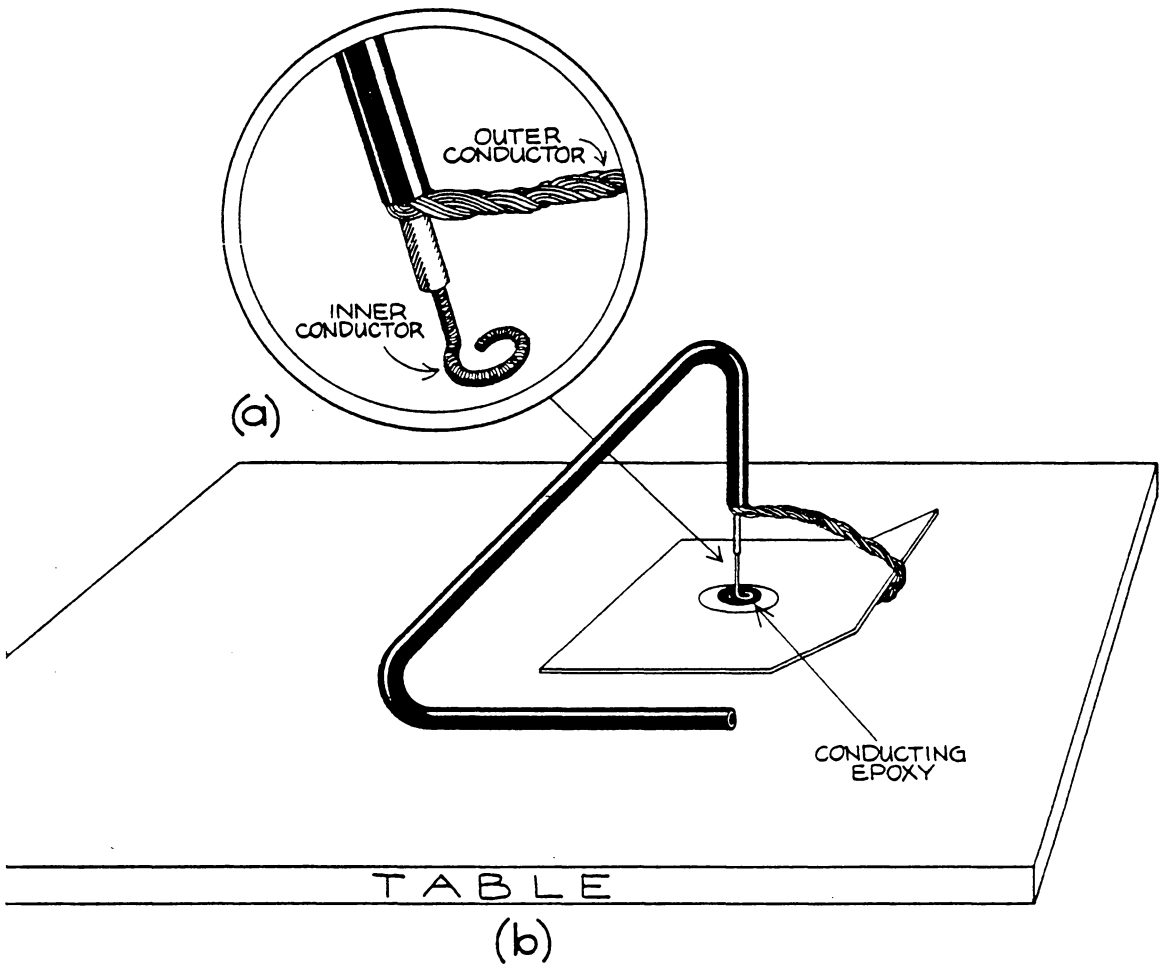

Figure 33. Cable Attachment: a) detail on end of cable, b) cable in dry position.

the 2 mm cast dries, the cable can be easily bent into position without the risk of breaking the connection. A second pouring is required to cast the cable in parallel with the front surface.

Any overnight non-conducting epoxy should suffice for the cast. Again, be sure to mix the epoxy for several minutes. This type of epoxy usually traps air bubbles which can be troublesome. To remove the air bubbles, place the mixed epoxy in a partial vacuum. This will cause the epoxy to "boil" away the trapped air. After degassing, gently pour the epoxy in the mold and let dry overnight. If the two level casting method is used, clean the the top of the first level with acetone before pouring the second layer. This will remove any waxes which might prevent bonding between the layers.

8. Finish

Remove the dried sensor from the mold by unscrewing the bolts and cutting the mylar. After removal, the sides and back of the cast should be filed flat and smoothly sanded. To improve noise immunity, coat the sensor with a thin coat of conductive epoxy. Polish the front surface smooth after the epoxy has dried overnight (at 70 degrees Celsius).

REFERENCES

[1] M. K. Brown, "A Controlled Impedance Gripper," AT&T Technical Journal, Vol. 64, No. 4, pp. 937-969.

[2] M. H. Raibert, and J. J. Craig, "Hybrid position/force control of manipulators," Trans. ASME, vol. 102, pp. 126-133, 1981.

[3] L. D. Harmon, "Automated Touch Sensing: A Brief Perspective and Several New Approaches," IEEE International Conference on Robotics, Atlanta, GA, March 13-15, 1982, pp. 326-331.

[4] W. D. Hillis, "A High Resolution Image Touch Sensor," The International Journal of Robotics, pp. 33-44, Vol. 1, No. 2, 1982.

[5] P. Dario and D. De Rossi, "Tactile Sensors and the Gripping Challenge," IEEE Spectrum, pp. 46-52, Vol. 22, No. 8, August 1985.

[6] P. Dario, D. De Rossi, C. Domenici, R. Francesconi, "Ferroelectric Polymer Tactile Sensors with Anthroporphic Features," IEEE International Conference on Robotics, Atlanta, GA, March 13-15, 1982, pp. 332-340.

[7] J. S. Schoenwald, "Strategies for Robotics Sensing Using Acoustics," Proceedings IEEE Ultrasonics Symposium, San Francisco, CA, Oct. 16-18, 1985.

[8] P. C. Chen, R. S. Muller, and R. M. White, "Thin Film ZnO-MOS Transducers With Virtually dc Response," Proceedings IEEE Ultrasonics Symposium, Nov. 1980.

[9] D. L. Polla, R. S. Muller, and R. M. White, "Pyroelectric Properties and Applications of Sputtered Zinc Oxide Thin Films," Proceedings IEEE Ultrasonics Symposium, San Francisco, CA, 1985.

[10] A. J. Bur and S. C. Roth, "Development of a Polymer Pressure Gage with Temperature Compensation," National Bureau of Standards Interim Report, Contact No. 82-64, 1982.

[11] Kynar Technical Manual, Pennwalt Corporation, 1983.

[12] Signetics Analog Applications Manual, Signetics Corporation, 1979.

[13] G. McPherson, An Introduction to Electric Machines and Transformers, New York: John Wiley & Sons, 1981.

[14] W. Sachse and N. N. Hsu, "Ultrasonic transducers for material testing and their characteristics," in Physical Acoustics, Vol. 14, W. P. Mason and R. N. Thuston, eds., New York: Academic Press, 1979.

Additional References

M. F. Barsky, D. K. Lindner, and R. O. Claus, "Active Damping of a Robot Gripper Using PVDF Piezoelectric Sensors," Proceedings of the Eighteenth Southeastern Symposium on System Theory, Knoxville, TN, April 7-8, 1986, pp. 418-422.

M. F. Barsky, D. K. Lindner, and R. O. Claus, "Robot Gripper Control System Using PVDF Piezoelectric Sensors," IEEE Transactions on Ultrasonics, Ferroelectrics, and Frequency Control, Nov. 1986.

B. C. Kuo, Automatic Control Systems, fourth edition, New Jersey: Prentice-Hall, 1982.

M. T. Mason and J. K. Salisbury, Jr., Robot Hands and the Mechanics of Manipulation, Cambridge: MIT Press, 1985.

The vita has been removed from the scanned document